

Robust Supermassive Black Hole Spin Mass-Energy Characteristics: A New Method and Results

Ruth A. Daly[★]

Penn State University, Berks Campus, Reading, PA 19608, USA

Accepted XXX. Received YYY; in original form ZZZ

ABSTRACT

The rotational properties of astrophysical black holes are fundamental quantities that characterize the black holes. A new method to empirically determine the spin mass-energy characteristics of astrophysical black holes is presented and applied here. Results are obtained for a sample of 100 supermassive black holes with collimated dual outflows and redshifts between about zero and two. An analysis indicates that about two-thirds of the black holes are maximally spinning, while one-third have a broad distribution of spin values; it is shown that the same distributions describe the quantity $(M_{\text{rot}}/M_{\text{irr}})$. The new method is applied to obtain the black hole spin mass-energy, M_{spin} , available for extraction relative to: the maximum possible value, the irreducible black hole mass, and the total black hole mass, M_{dyn} . The total energy removed from the black hole system and deposited into the circumgalactic medium via dual outflows over the entire outflow lifetime of the source, E_{T} , is studied relative to M_{dyn} and relative to the spin energy available per black hole, $E_{\text{spin}}/(M_{\odot}c^2)$. The mean value of $\text{Log}(E_{\text{T}}/M_{\text{dyn}})$ is about (-2.47 ± 0.27) . Several explanations of this and related results are discussed. For example, the energy input to the ambient gas from the outflow could turn off the accretion, or the impact of the black hole mass loss on the system could destabilize and terminate the outflow. The small values and restricted range of values of $\text{Log}(E_{\text{T}}/M_{\text{dyn}})$ and $\text{Log}(E_{\text{T}}/E_{\text{spin}})$ could suggest that these are fundamental properties of the primary process responsible for producing the dual collimated outflows.

Key words: black hole physics – galaxies: active – methods: analytical – quasars: supermassive black holes – gravitation

1 INTRODUCTION

Black holes are ubiquitous in the universe. Supermassive black holes reside at the centers of galaxies and stellar-mass black holes populate galaxies. The two primary characteristics that describe an astrophysical black hole are the mass and spin of the hole (assuming the black hole has negligible charge). Often in astrophysical contexts, the mass of a black hole is empirically determined by the dynamics and properties of matter and light in the vicinity of the black hole. The black hole mass that will be measured is the total black hole mass, M , which has contributions from the irreducible mass, M_{irr} , and the mass-energy associated with the spin angular momentum of the black hole J : $M = (M_{\text{irr}}^2 + (Jc/(2GM_{\text{irr}}))^2)^{1/2}$, where G is the gravitational constant and c is the speed of light (e.g. Christodoulou 1970; Bardeen, Press, & Teukolsky 1972; Misner, Thorne, & Wheeler 1973; Rees 1984; Blandford 1990); this equation may be rewritten in the form of eqs. (3) and (9). The mass-energy that can be extracted from the spinning black hole, referred to here as the "spin mass-energy," is $M_{\text{spin}} = M - M_{\text{irr}}$,

as described in detail by Thorne et al. (1986) (see their eq. 3.88 and related discussion). Thus, there are two different quantities that have been referred to as spin or rotational mass-energy of the black hole in the literature (e.g. Rees 1984; Thorne et al. 1986; Gerosa, Fabbri, & Sperhake 2022). For clarity, throughout this paper, the quantity $M_{\text{rot}} \equiv Jc/(2GM_{\text{irr}})$ is referred to as the "rotational mass." The quantity $M_{\text{spin}} \equiv M - M_{\text{irr}} \equiv E_{\text{spin}}c^{-2}$ is referred to as the "spin mass-energy" of the black hole and indicates the mass-energy that is available to be extracted from the black hole (see, for example, Blandford & Znajek 1977; Rees 1984; Thorne et al. 1986, and Blandford 1990 for detailed discussions). The mass, M , is also referred to as the dynamical mass, M_{dyn} , since it is the total black hole mass that will be inferred by dynamical and other astronomical studies.

The irreducible mass of an isolated black hole can not be reduced or decreased, but mass-energy associated with black hole spin can be extracted, thereby decreasing the total mass of the hole (Penrose 1969; Penrose & Floyd 1971; Blandford & Znajek 1977). Collimated outflows from supermassive black holes associated with active galactic nuclei (AGN) and stellar-mass black holes associated with X-ray binaries are likely to be powered, at least in part, by

[★] E-mail: rdaly@psu.edu

black hole spin (e.g. Blandford & Znajek 1977; MacDonald & Thorne 1982; Phinney 1983; Begelman, Blandford, & Rees 1984; Blandford 1990; Daly 1994, 1995; Moderski, Sikora, & Lasota 1998; Meier 1999; Koide et al. 2000; Wan et al. 2000; Punsly 2001; Daly & Guerra 2002; De Villiers, Hawley, & Krolik 2003; Gammie et al. 2004; Komissarov & McKinney 2007; Beckwith, Hawley, & Krolik 2008; King, Pringle, & Hofmann 2008; Miller et al. 2009; O’Dea et al. 2009; Daly 2009a,b; Tchekhovskoy et al. 2010; Daly 2011; Gnedin et al. 2012; King et al. 2013; Ghisellini et al. 2014; Yuan & Narayan 2014; Daly & Sprinkle 2014; Daly 2016; Gardner & Done 2018; Krause et al. 2019; Reynolds 2019; Daly 2019). In this case, the spin energy extracted during the outflow will cause the black hole mass to decrease. A source that undergoes multiple outflow events could significantly drain the spin energy of the hole and thereby decrease the black hole mass. The amount of spin energy extracted during outflow events have been estimated for radio sources with large-scale outflows such as FRI sources in galaxy-cluster environments (McNamara et al. 2009; Daly 2009a,b, 2011), FRII sources (Daly 2009a,b; 2011), and several types of AGN and stellar-mass black holes (Daly 2020). FRI sources are extended radio sources that are "edge-darkened" while FRII sources, also known as classical doubles, are "edge-brightened" (Fanaroff & Riley 1974). In addition, the fraction of the spin energy extracted per outflow event has been estimated for FRII sources (Daly 2011), and is roughly a few to several percent. Thus, in models in which collimated outflows from the vicinity of a black hole are powered by black hole spin, the spin and spin-energy of the hole are expected to decrease as a result of the outflow.

The fact that the mass-energy associated with black hole spin may be extracted, modified, or reduced, and thus that the total or dynamical mass of a black hole can be reduced may introduce dispersion in relationships between black hole mass and properties of the host galaxy (e.g. Kormendy & Richstone 1995; Ferrarese & Ford 2005; Kormendy & Ho 2013; Shankar 2013; Sesana et al. 2014; Zubovas & King 2019; King & Nealon 2019; King & Pounds 2015). If black hole spin evolves with redshift, this is likely to cause an evolution in these relationships and their dispersion. Additionally, black hole spin is expected to evolve with redshift as a result of the merger and accretion history of the black hole (e.g. Hughes & Blandford 2003; Gammie et al. 2004; Volonteri et al. 2005, 2007; King & Pringle 2006, 2007; King et al. 2008; Berti & Volonteri 2008; Ghisellini et al. 2013). Thus, the study of black hole spin evolution provides insight into the merger and accretion history of supermassive black holes. Black hole spin may depend upon galaxy type or environment (e.g. Sesana et al. 2014; Antonini et al. 2015; King & Pounds 2015; Barausse et al. 2017; King & Nealon 2019), which may lead to environmental changes in the relationship between black hole mass and galaxy properties, or a change in the dispersion of relationships (e.g. Zubovas & King 2012). The dispersion introduced may be complex and will depend upon the initial spin and irreducible mass of the black hole, the processes responsible for spinning up the hole such as accretion or mergers, processes which tap or reduce the spin of the hole, and the complex interaction of feedback, accretion, outflows, and other processes associated with the black hole, which are likely to play a role in determining the spin and thus spin mass-energy and dynamical mass of the hole (e.g. Belsole et al. 2007; Worrall 2009; Voit et al. 2015; Hardcastle & Croston 2020). In addition, it is likely that some sources undergo multiple outflow events (e.g. Hardcastle et al. 2019; Bruni et al. 2019, 2020; Shabala et al. 2020), so that even if a small amount of the spin energy is extracted per outflow event,

over time a substantial amount of spin energy can be extracted due to multiple outflow events.

The distinction between dynamical mass, spin mass-energy, and irreducible mass of a black hole is also important when comparing empirically determined quantities with theoretically predicted quantities, such as those indicated by numerical simulations. Numerical simulations predict the expected black hole spin and mass evolution in the context of different black hole merger and accretion histories (e.g. King et al. 2008; Volonteri et al. 2013; Dubois, Volonteri, & Silk 2014; Sesana et al. 2014; Kulier et al. 2015). A comparison of simulation results with empirically determined results provides an important diagnostic of the merger and accretion histories of black holes located at the centers of galaxies.

The number of available black hole spin values, and therefore black hole spin energies, has recently increased substantially. The development of the "outflow method" of empirically determining black hole spin and accretion disk properties developed and described by Daly (2016) and Daly (2019) (hereafter D16 and D19) and Daly et al. (2018), allow the empirical determination of the black hole spin function, spin, and, accretion disk properties such as the mass accretion rate and disk magnetic field strength for over 750 sources. D19 showed that the fundamental equation that describes an outflow powered at least in part by black hole spin, $L_j \propto B_p^2 M_{\text{dyn}}^2 F^2$ (e.g. Blandford & Znajek 1977; Meier 1999; Tchekhovskoy et al. 2010; Yuan & Narayan 2014) is separable and may be written as

$$(L_j/L_{\text{Edd}}) = g_j (B/B_{\text{Edd}})^2 F^2 \quad (1)$$

(see eq. 6 from D19); here B_p is the poloidal component of the accretion disk magnetic field, B is the magnitude of disk magnetic field, B_{Edd} is the Eddington magnetic field strength (e.g. Rees 1984; Blandford 1990; Dermer et al. 2008; D19), $B_{\text{Edd}} \approx 6 \times 10^4 (M_{\text{dyn}}/10^8 M_{\odot})^{-1/2} \text{ G}$, $F^2 \equiv f(j)/f_{\text{max}}$ is the normalized spin function (discussed in more detail in section 2), f_{max} is the maximum value of the spin function $f(j)$, and g_j is the normalization factor for the beam power L_j in units of the Eddington Luminosity, L_{Edd} , $(L_j/L_{\text{Edd}})(\text{max}) = g_j$. Note that the ratio $(B_p/B)^2$ is absorbed into the normalization factor g_j , thus g_j may depend upon AGN type, as discussed in sections 3.1 and 4 of D19. (Also note that even though the maximum value of the spin function $f(j=1) = f_{\text{max}} = 1$, the normalization term f_{max} is included in eqs. (1) and (7) for completeness since in some numerical simulations $f(j)$ is described by modified representations (e.g. Tchekhovskoy et al. 2010). Here, since $f_{\text{max}} = 1$, the terms "spin function" and "normalized spin function" are used interchangeably.)

The spin functions obtained by D19 were converted to dimensionless black hole spin angular momentum values, and compared with values obtained with independent methods such as those discussed by Azadi et al. (2020) and Reynolds (2019); see also, for example, Gnedin et al. (2012), Patrick et al. (2012), King et al. (2013), Walton et al. (2013), Wang et al. (2014), García et al. (2015), Mikhailov et al. (2015, 2019), Vasudevan et al. (2016), Piotrovich et al. (2017, 2020), and Mikhailov & Gnedin (2018). A comparison of black hole spin parameters obtained independently with the outflow method and the continuum fitting method was possible for 15 of the sources studied with both methods (Azadi et al. 2020), and consistent spin parameters were obtained with the two methods. And, a comparison was possible and very good agreement was found for six AGN and one stellar mass black hole studied with both the outflow method and the X-ray reflection method (e.g. Fabian et al. 1989; Iwasawa et al. 1997; Miller et al. 2002; Reynolds 2019), which included all of the sources for which a comparison

is currently possible. Thus, all sources for which independent spin angular momentum values could be compared indicate good agreement between independently determined values. The high spin values obtained are also consistent with expectations based on AGN luminosities (e.g. Sun & Malkan 1989; Davis & Laor 2011; Wu et al. 2013; Trakhtenbrot 2014; Brandt & Alexander 2015; Trakhtenbrot, Volonteri, & Natarajan 2017). So, the expectation is that some significant fraction of black holes are likely to have high spin; there may also be a population of black holes with lower spin, and, of course, black hole spin is likely to be an evolving quantity.

Here, a new method to study the spin mass-energy characteristics of black holes is presented and applied to a sample of 100 supermassive black holes with empirically determined black hole spin functions. This is important because the spin mass-energy of a black hole can be extracted, thereby reducing the total black hole mass, and energy channelled away from the hole can significantly impact the near and far field environments of the black hole. The traditional and new methods of empirically determining the spin mass-energy characteristics of black holes are described in sections 2.1 and 2.2, respectively.

Empirically determined spin functions, F^2 , are used to obtain the spin mass-energy characteristics of the sample of 100 supermassive black holes, bypassing the use of dimensionless spin angular momenta, j . The properties of the spin functions (see eq. 7) are described and analyzed in section 2.3, and it is found that the sources are well described by a population of maximally spinning black holes plus a population of holes with a broad distribution of spin values. In section 3, the empirically determined spin functions are applied to obtain for each black hole: the spin mass-energy relative to the maximum possible value; the spin mass-energy relative to the irreducible and dynamical black hole mass; the spin mass-energy in units of solar masses; the ratio of the total outflow energy to the black hole spin energy; the ratio of the total outflow energy to the dynamical black hole mass; and the ratios of the rotational mass relative to the irreducible and dynamical black hole masses. The results are discussed and summarized in sections 4 and 5.

All quantities are obtained in a spatially flat cosmological model with two components, a mean mass density relative to the critical value at the current epoch of $\Omega_m = 0.3$ and a similarly normalized cosmological constant of $\Omega_\Lambda = 0.7$. A value for Hubble's constant of $H_0 = 70 \text{ km s}^{-1} \text{ Mpc}^{-1}$ is assumed throughout.

2 METHOD

The traditional method of obtaining black hole spin mass-energy characteristics and some of the difficulties that arise in the application of this method to empirically determine spin mass-energy properties of astrophysical black holes are described in section 2.1. The new method avoids these difficulties by characterizing the spin mass-energy characteristics in terms of the spin function; the new method that will be applied here is presented in section 2.2. The properties of the empirically determined spin functions that will be applied to obtain and study the spin mass-energy characteristics of 100 supermassive black holes are discussed in section 2.3.

2.1 The Traditional Method

As described in section 1, the rotational energy of a black hole contributes to the total dynamical black hole mass, M_{dyn} , which is the mass that will be measured by a distant observer, and $M_{\text{dyn}}^2 = M_{\text{irr}}^2 + M_{\text{rot}}^2$ (see eq. 3), where $M_{\text{rot}} \equiv (Jc/(2GM_{\text{irr}}))$. The

spin energy E_{spin} that may be extracted is $E_{\text{spin}} = M_{\text{spin}}c^2$, where $M_{\text{spin}} = M_{\text{dyn}} - M_{\text{irr}}$, and is referred to here as the black hole spin energy or spin mass-energy.

Relationships between the dimensionless black hole spin angular momentum, j , the total black hole mass, M (also referred to as M_{dyn}), and the mass-energy that can be extracted from the black hole, M_{spin} , are discussed, for example, by Misner, Thorne, & Wheeler (1973), Rees (1984), Blandford (1990), and Thorne et al. (1986). The dimensionless black hole spin angular momentum j is defined in the usual way in terms of the spin angular momentum J and the total black hole mass M , $j \equiv Jc/(GM^2)$; in other work, j is sometimes represented with the symbol a_* or a/M . As described in section 1, the work of Thorne et al. (1986) (see also Rees 1984; Blandford 1990), indicates the following set of equations:

$$M \equiv M_{\text{dyn}} = M_{\text{irr}} + E_{\text{spin}}c^{-2} = M_{\text{irr}} + M_{\text{spin}} \quad (2)$$

and

$$M_{\text{irr}} = M_{\text{dyn}} \left(\frac{1 + (1 - j^2)^{1/2}}{2} \right)^{1/2}, \quad (3)$$

where eq. (3) follows from $M_{\text{dyn}}^2 = M_{\text{irr}}^2 + (Jc/(2GM_{\text{irr}}))^2$, discussed in section 1. Eqs. (2) and (3) indicate that

$$\frac{M_{\text{spin}}}{M_{\text{dyn}}} = 1 - \left(\frac{M_{\text{irr}}}{M_{\text{dyn}}} \right) \quad (4)$$

and

$$\frac{M_{\text{spin}}}{M_{\text{irr}}} = \left(\frac{M_{\text{dyn}}}{M_{\text{irr}}} \right) - 1. \quad (5)$$

Eqs. (3) & (5) indicate that

$$\frac{E_{\text{spin}}}{E_{\text{spin,max}}} = \left(\frac{\sqrt{2}(1 + \sqrt{1 - j^2})^{-0.5} - 1}{\sqrt{2} - 1} \right) \approx 2.41 \left(\frac{M_{\text{spin}}}{M_{\text{irr}}} \right), \quad (6)$$

where $(E_{\text{spin}}/E_{\text{spin,max}})$ is obtained by dividing eq. (5) as a function of j by eq. (5) with $j = 1$, since $(E_{\text{spin,max}}/M_{\text{irr}})$ is obtained with eqs. (3) and (5) assuming a value of $j = 1$.

There are several factors that indicate it is preferable to rewrite equations (3 - 5) in terms of the spin function $F^2 \equiv f(j)/f_{\text{max}}$. In the application of the outflow method (D16, D19), the quantity that is determined empirically is F , so it is preferable to be able to obtain the quantities on the left hand sides of equations (3-6) directly in terms of F , where

$$F \equiv \sqrt{\frac{f(j)}{f_{\text{max}}}} = \frac{j}{(1 + \sqrt{1 - j^2})}. \quad (7)$$

To further complicate the use of j to empirically characterize the spin properties of a black hole, the quantity $\sqrt{1 - j^2}$ indicates that values of j that are greater than one cannot be accommodated, though the uncertainties associated with empirically determined black hole spin characteristics should allow for this possibility (e.g. Daly 2020). In addition, the relationship between the normalized spin energy of the black hole and the dimensionless spin angular momentum j is highly non-linear as indicated by eq. (6) and illustrated by Fig. 1. The spin energy $E_{1/2}$ is about half of the maximum possible spin energy for j of about 0.9; the spin energy $E_{1/4}$ is about one quarter of the maximum value when j is about 0.7; and the spin energy $E_{1/10}$ is about one tenth of the maximum value when j is about 0.5. It is clear that the relationship between the normalized spin energy and j is quite non-linear, and relatively high dimensionless spin angular momentum values of 0.5 and 0.7

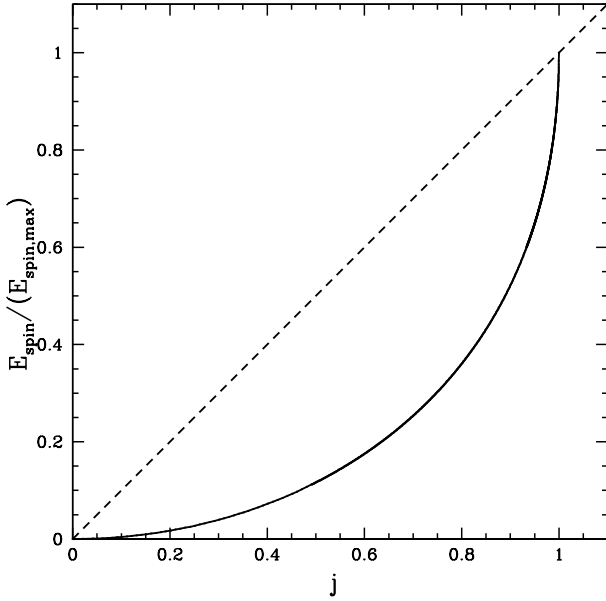


Figure 1. The solid line shows the black hole spin energy available for extraction, E_{spin} in units of the maximum possible value of this energy, $E_{\text{spin,max}}$, versus the dimensionless black hole spin angular momentum j (defined in section 2.1). The dotted line provides a comparison to a linear relationship.

indicate relatively low spin energy values of only 1/10 and 1/4, respectively, of the maximum possible value. Another way to state this is that relatively low values of spin energy indicate substantial values of dimensionless black hole spin angular momentum j . Thus, if a black hole has any spin energy at all, it is expected to have a value of j substantially different from zero.

The facts that the relationship between the dimensionless spin angular momentum j and the normalized spin energy ($E_{\text{spin}}/E_{\text{spin,max}}$) is highly non-linear, that empirically determined values of j cannot exceed unity due to the term $\sqrt{1-j^2}$ even though observational uncertainties require this flexibility, and that the empirically determined quantity is F , suggest that some other function should be used to empirically determine the spin mass-energy properties of black holes. And, as noted earlier, it is important to determine how much of the dynamical mass could be extracted and thereby decrease the black hole mass. Spin energy also indicates the potential impact of the "spin energy reservoir" that is stored in spinning black holes on the near and far field environments of black holes.

2.2 The New Method

In contradistinction to these issues, the relationship between both the black hole spin function F , F^2 , or $\text{Log}(F)$ and the black hole mass-energy associated with the spin do not suffer from the limitations described in section 2.1, as illustrated in Figs. 2, 3, and 4. Though theoretically F is not expected to exceed unity, empirically determined values of F will exceed unity due to measurement uncertainties. There are several additional reasons why it is preferable to use the quantity F , F^2 , or $\text{Log}(F)$: (1) there is no mathematical constraint analogous to that for j (described in section 2.1) that requires that F must be less than or equal to one; (2) the relationship between F and spin energy is only slightly non-linear as illustrated in Fig. 2;

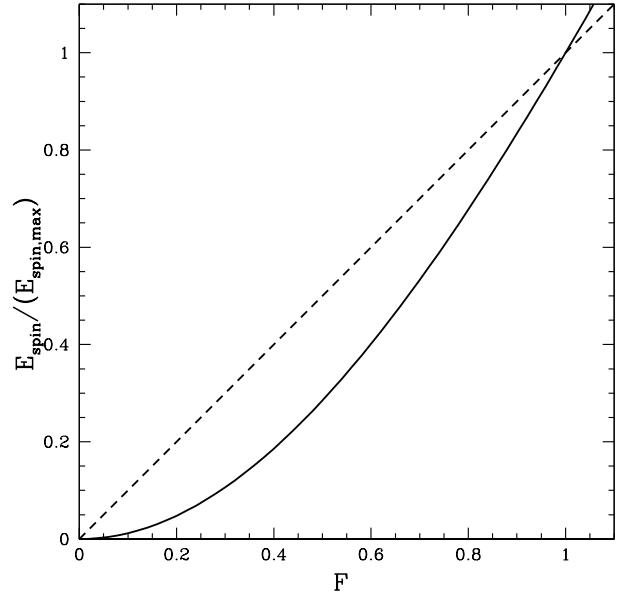


Figure 2. The solid line shows the available black hole spin energy E_{spin} normalized to the maximum possible value of the spin energy, $E_{\text{spin,max}}$, as a function of F , the square root of the black hole spin function (defined by eq. 7). The dotted line provides a comparison to a linear relationship.

(3) the spin energy in units of the maximum spin energy is very well approximated by the value of F^2 for values of F^2 between about zero and 1.5 or so as illustrated in Fig. 3. Allowing the exponent of F to vary, it is found that $\text{Log}(E_{\text{spin}}/E_{\text{spin,max}}) \approx 1.75 \text{Log}(F)$, as illustrated in Fig. 4. It should be noted that equations (9-12) should be used to obtain uncertainties for $(M_{\text{irr}}/M_{\text{dyn}})$, $(M_{\text{spin}}/M_{\text{dyn}})$, $(M_{\text{spin}}/M_{\text{irr}})$, $(E_{\text{spin}}/E_{\text{spin,max}})$ and related quantities, which are listed below.

To re-write equations (3-6) in terms of F , we manipulate the relationship between F and j obtained and discussed by D19 to obtain

$$0.5 [1 + (1 - j^2)^{1/2}] = (F^2 + 1)^{-1}. \quad (8)$$

This is then substituted into eq. (3) to obtain:

$$\frac{M_{\text{irr}}}{M_{\text{dyn}}} = (F^2 + 1)^{-1/2}. \quad (9)$$

Combining eqs. (2) and (9) indicates that

$$\frac{M_{\text{spin}}}{M_{\text{dyn}}} = 1 - \left(\frac{M_{\text{irr}}}{M_{\text{dyn}}} \right) = [1 - (F^2 + 1)^{-1/2}], \quad (10)$$

and

$$\frac{M_{\text{spin}}}{M_{\text{irr}}} = \left(\frac{M_{\text{dyn}}}{M_{\text{irr}}} \right) - 1 = [(F^2 + 1)^{1/2} - 1]. \quad (11)$$

Eq. (11) indicates that

$$\frac{E_{\text{spin}}}{E_{\text{spin,max}}} = \frac{M_{\text{spin}}}{M_{\text{spin,max}}} = \left(\frac{\sqrt{F^2 + 1} - 1}{\sqrt{2} - 1} \right) \approx 2.41 \left(\frac{M_{\text{spin}}}{M_{\text{irr}}} \right) \quad (12)$$

where $(E_{\text{spin}}/E_{\text{spin,max}})$ is obtained by dividing eq. (11) as a function of F by eq. (11) with $F = 1$, since $(E_{\text{spin,max}}/M_{\text{irr}})$ is obtained with eqs. (9) and (11) assuming a value of $F = 1$.

Equations (9-12) will be applied to empirically determine the ratio of the dynamical black hole mass to the irreducible black

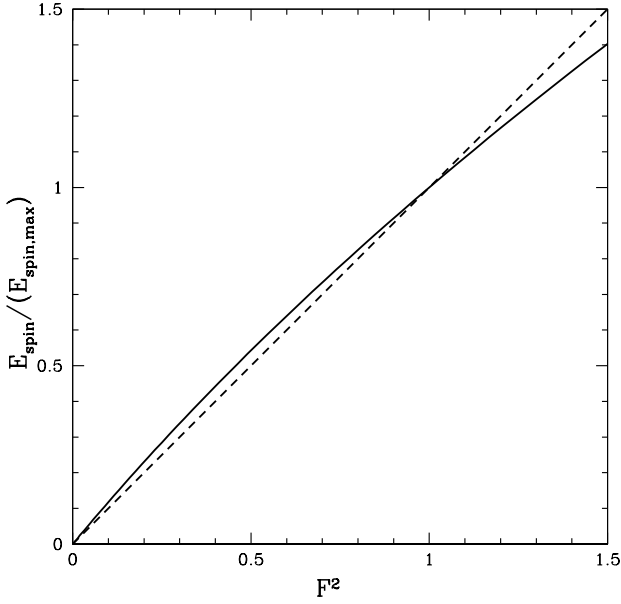


Figure 3. The solid line shows the available black hole spin energy E_{spin} normalized to the maximum possible value of this spin energy, $E_{\text{spin,max}}$, as a function of the black hole spin function, F^2 (defined by eq. 7). The dotted line provides a comparison to a linear relationship.

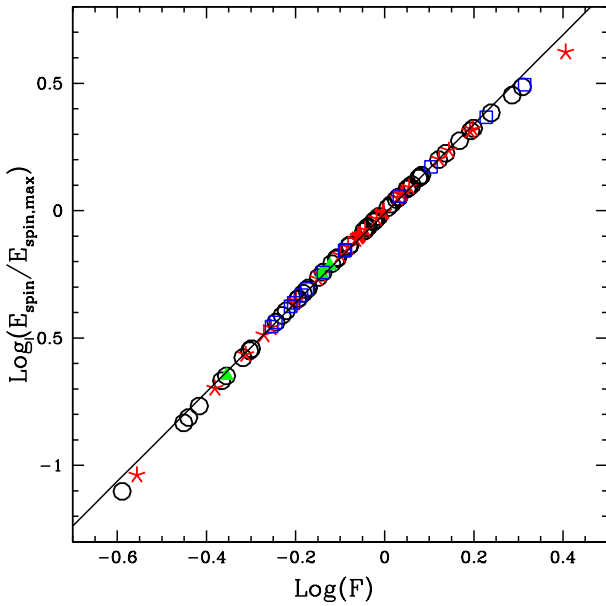


Figure 4. $\text{Log}(E_{\text{spin}}/E_{\text{spin,max}})$ as a function of the $\text{Log}(F)$ is illustrated with input values of $\text{Log}(F)$ selected to match those of the 100 FR II sources that will be considered here, but the input values of $\text{Log}(F)$ could have been selected as in Figs. 2 and 3. The unweighted best fit line (solid line) has a slope of 1.75 ± 0.01 , y-intercept of -0.011 ± 0.002 , and $\chi^2 = 0.03$. Here the exponent that F is raised to is allowed to vary, while in Fig. 3 this exponent is fixed. The symbols and colors are as in Fig. 6.

hole mass, $M_{\text{dyn}}/M_{\text{irr}}$, the ratio of the spin mass-energy to the dynamical mass $M_{\text{spin}}/M_{\text{dyn}}$, the ratio of the spin mass-energy to the irreducible black hole mass $M_{\text{spin}}/M_{\text{irr}}$, and the spin energy in terms of the maximum spin energy, $E_{\text{spin}}/E_{\text{spin,max}}$ for a sample of 100 FR II sources. Of course, the maximum value of M_{spin} obtained from eqs. (10) and (11) with $F = 1$, remain $(M_{\text{spin}}/M_{\text{dyn}})_{\text{(max)}} \approx 0.29$ and $(M_{\text{spin}}/M_{\text{irr}})_{\text{(max)}} \approx 0.41$, while the maximum value of $(M_{\text{dyn}}/M_{\text{irr}})$ obtained with $F = 1$ (or $j = 1$) is $\sqrt{2}$.

Eqs. (9-12) indicate the following uncertainties: $\delta(M_{\text{dyn}}/M_{\text{irr}}) = F[(F^2 + 1)^{-0.5}] \delta F$; $\delta(M_{\text{spin}}/M_{\text{dyn}}) = F[(F^2 + 1)^{-1.5}] \delta F$; $\delta(M_{\text{spin}}/M_{\text{irr}}) = \delta(M_{\text{dyn}}/M_{\text{irr}})$, and $\delta(E_{\text{spin}}/E_{\text{spin,max}}) = F(F^2 + 1)^{-0.5}(\sqrt{2} - 1)^{-1} \delta F$. Of course, $\delta(\text{Log}(x)) = (\delta(x)/x)/\ln(10)$. These uncertainties are included in the Tables and shown in plots of quantities versus redshift.

The total mass-energy associated with the spin of the black hole can be obtained by multiplying $(M_{\text{spin}}/M_{\text{dyn}})$ by the empirically determined mass of the black hole, M . This is the first time the empirically determined black hole mass is required. Clearly,

$$\frac{E_{\text{spin}}}{(M_{\odot}c^2)} = \frac{M_{\text{spin}}}{M_{\odot}} = M \times \left(\frac{M_{\text{spin}}}{M_{\text{dyn}}} \right). \quad (13)$$

All empirically determined black hole masses are dynamical black hole masses. This will be discussed in more detail in section 4. Empirically determined black hole masses and their uncertainties are indicated by the Eddington luminosities listed in D16 & D19.

The rotational mass, defined and described in section 1, can also be represented in terms of the spin function, F^2 . It is easy to show that

$$\frac{M_{\text{rot}}}{M_{\text{irr}}} = F \quad (14)$$

and

$$\frac{M_{\text{rot}}}{M_{\text{dyn}}} = \frac{F}{\sqrt{F^2 + 1}}. \quad (15)$$

Each of these quantities can easily be obtained for the 100 sources studied here from Tables 1 and 2, given that $\text{Log}(M_{\text{rot}}/M_{\text{irr}}) = \text{Log}(F)$ and $\text{Log}(M_{\text{rot}}/M_{\text{dyn}}) = [\text{Log}(F) - \text{Log}(M_{\text{dyn}}/M_{\text{irr}})]$, as discussed in section 4.1.

2.3 Properties of the Spin Function

Spin functions, F^2 , for the 100 supermassive black holes associated with FR II sources obtained by D19 are considered here. The values of $\text{Log}(F)$ and their uncertainties are listed in Tables 1 and 2, and a histogram of values is shown in Fig. 5. The sources are drawn from the flux limited 3CRR catalogue of radio sources (Laing, Riley & Longair 1983), and thus are subject to well-known selection effects such as the loss of lower-luminosity sources as source redshift increases (e.g. see Fig. 1 of McLure et al. 2004). To illustrate the impact of this selection effect on the histogram of each quantity, the redshift distribution of each quantity is provided and discussed; for example, the redshift distribution of $\text{Log}(F)$ is shown in Fig. 6, and will be discussed below.

The values of $\text{Log}(F)$ are illustrated with the histogram shown in Fig. 5. The bin size in this and all subsequent histograms is selected to be close to the mean value of the uncertainty for the quantity displayed. A maximally spinning black hole is expected to have a value of $\text{Log}(F) = 0$, and sources that are not maximally spinning are expected to have values of $\text{Log}(F) < 0$. There are several sources with values of F greater than one, or $\text{Log}(F)$ greater than zero. To see if the number of such sources is similar to that

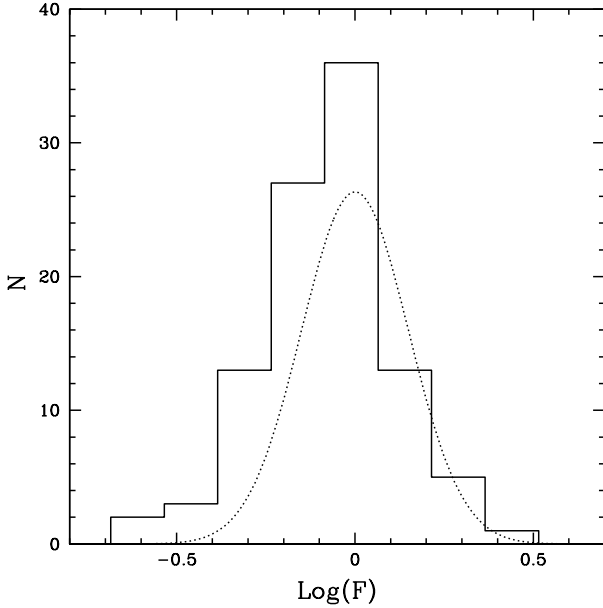


Figure 5. The histogram of $\text{Log}(F)$ is shown as the solid line. The population is well described with a two component model: a population of maximally spinning black holes with $\text{Log}(F) = 0$ and standard deviation $\sigma = 0.15$, illustrated by the Gaussian (dotted line), plus a population with $-0.6 < \text{Log}(F) < 0$ with a tilted distribution (see section 2.3). Of the sample of 100 black holes studied, about 2/3 are maximally spinning, and about 1/3 have a slowly declining distribution of spin functions toward lower values of $\text{Log}(F)$. $\text{Log}(M_{\text{rot}}/M_{\text{irr}}) = \text{Log}(F)$ (see eq. 14), so this is also the distribution of the values of $\text{Log}(M_{\text{rot}}/M_{\text{irr}})$. For all histograms, the bin size is selected to be close to the mean value of the uncertainty of the quantity listed in Tables 1 and 2.

expected given the mean uncertainty of $\delta\text{Log}(F) = 0.15$ per source for the sources listed in Tables 1 and 2, consider dividing the sources into two populations: those that are maximally spinning, and thus have $\text{Log}(F) = 0$, and a second population with some distribution of $\text{Log}(F)$, all of which have $\text{Log}(F)$ less than zero.

The population of maximally spinning sources is illustrated with a Gaussian distribution centered on $\text{Log}(F) = 0$, with a standard deviation equal to the mean uncertainty per source, $\sigma = 0.15$, and the peak height is determined by the number of sources that are maximally spinning (and it is determined below that about 66 of the 100 sources fall into this category) so the maximum height of the Gaussian is $66/\sqrt{(2\pi)}$, as illustrated with the dotted line in Fig. 5. This Gaussian provides a good description of the sources with $\text{Log}(F) > 0$, and the properties of the second population can be deduced by assuming the population of maximally spinning holes is symmetric about $\text{Log}(F) = 0$ and subtracting this population from the total number of sources. There are 22 sources with $0 \leq \text{Log}(F) \leq 0.15$, which indicates that for a population of sources with an intrinsic value of $\text{Log}(F) = 0$ and a Gaussian distribution of uncertainties we expect there to be about nine sources with $0.15 \leq \text{Log}(F) \leq 0.3$ $\text{Log}(F)$, and about one with $0.3 \leq \text{Log}(F) \leq 0.45$. For the sample studied here, there are ten sources between $+1$ and $+2$ σ for $\text{Log}(F) > 0$ (including the two sources with $\text{Log}(F) \approx 0.31$ with this group), one source between $+2$ and $+3$ σ , and zero sources that deviate by more than $+3$ σ . This is just about as expected for a population of sources centered at $\text{Log}(F) = 0$ with $\sigma \approx 0.15$.

Extending this to the sources with $\text{Log}(F) < 0$, we can obtain

the number of sources over and above that expected based on a symmetric distribution about $\text{Log}(F) = 0$ of the population of maximally spinning black holes to study the properties of the second population of sources. This indicates that, over and above the sources expected from the Gaussian distribution (based on the numbers listed above), there are 13 additional sources with $-0.15 \leq \text{Log}(F) < 0$, 11 additional sources with $-0.3 \leq \text{Log}(F) < -0.15$, and ten additional sources with $-0.6 < \text{Log}(F) < -0.3$, for a total of 34 sources above those expected from the Gaussian distribution. This suggests that the sources studied here consist of two populations: a single population of maximally spinning black holes with $\text{Log}(F) = 0$ and $\sigma(\text{Log}(F)) = 0.15$ with a total of 66 sources, plus another population that has a tilted distribution in $\text{Log}(F)$, all of which have $-0.6 \leq \text{Log}(F) < 0$, with a total of 34 sources.

The number of sources per unit $\text{Log}(F)$ in this second population is about 90 for $-0.15 \leq \text{Log}(F) < 0$, about 70 for $-0.3 \leq \text{Log}(F) < -0.15$, and about 30 for the remainder of the sources, which have $-0.6 < \text{Log}(F) < -0.3$. Part or all of this decline in the number of sources per unit $\text{Log}(F)$ as $\text{Log}(F)$ decreases could be due to observational selection effects, although part could be due to an intrinsic decline.

These values indicate that about two-thirds of the sample of 100 supermassive black holes are maximally spinning and are described by a Gaussian distribution about $\text{Log}(F) = 0$ with $\sigma \approx 0.15$. About one-third of the sample are less than maximally spinning and have a tilted distribution of spin functions, with the $\text{Log}(F)$ ranging from about $(-0.6$ to $0)$, with the number of sources per unit $\text{Log}(F)$ declining as $\text{Log}(F)$ decreases, as illustrated in Fig. 5.

The redshift distribution of $\text{Log}(F)$ is shown in Fig. 6. The FRII radio sources are categorized based on their spectroscopic nuclear properties. The sample considered here includes high excitation galaxies (HEG), low excitation galaxies (LEG), quasars (Q), and weak sources (W) and each type is represented by a different color; the classifications listed here were obtained from Grimes et al. (2004). An unweighted fit is provided, and the fitted parameters are summarized in Table 3. It is clear from Fig. 6 that sources with low values of $\text{Log}(F)$ drop out of the sample as redshift increases. This is because sources with lower radio luminosity have lower beam power and thus lower values of $\text{Log}(F)$; the beam power is discussed in more detail in section 4.3 (see also D16 and D19). The radio selection effect that causes sources with lower radio luminosity to drop out of the sample as redshift increases causes sources with lower values of $\text{Log}(F)$ to drop out of the sample as redshift increases.

Thus, supermassive black holes with a broad range of values of $\text{Log}(F)$ are present at low redshift, while those with low values of $\text{Log}(F)$ drop out as redshift increases from zero to two. This selection effect causes a dearth of sources with low values of F or $\text{Log}(F)$ at high redshift, which is clearly evident in Figs. 5 and 6, and is due to the flux-limited nature of the survey from which the sources studied here are drawn. This same selection effect is also apparent in all of the quantities that depend only upon $\text{Log}(F)$.

3 RESULTS

The data for a sample of 100 FRII sources presented and discussed by D16 & D19 are considered and applied here. The results are listed in Tables 1 and 2, and summarized in Table 3, where the typical uncertainty per source of each quantity is included in (brackets). Full details obtained with high excitation radio galaxies (HEG) are included in Table 1 while those obtained with low excitation galaxies

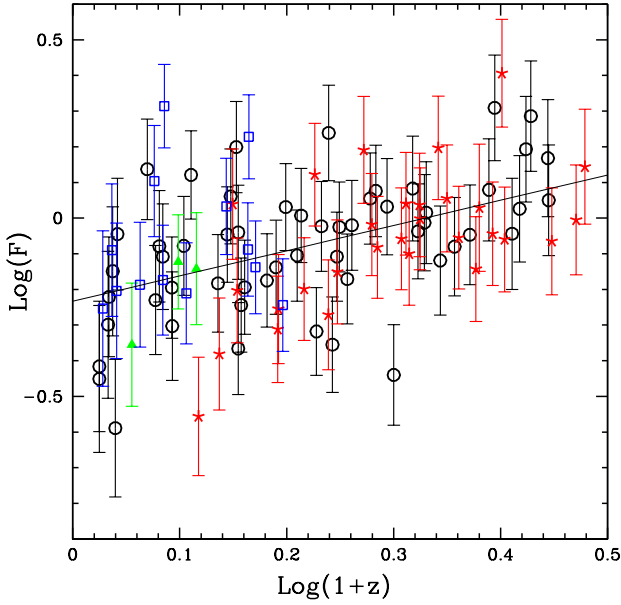


Figure 6. The redshift (z) distribution of $\text{Log}(F)$ is shown here. The theoretically expected maximum value of this quantity is 0. In this and all similar figures, HEG are denoted by open black circles, Q are denoted by red stars, LEG are denoted by blue squares, and W are denoted by green triangles. The parameters describing the best fit line in this and all similar figures are listed in Table 3; all fits are unweighted. This is also the redshift distribution for the quantity $\text{Log}(M_{\text{rot}}/M_{\text{irr}})$ (see eq. 14).

(LEG), radio loud quasars (Q), and weak sources (W) (as defined by Grimes et al. 2004) are listed in Table 2. Included in Tables 1 and 2 are the $\text{Log}(F)$ values obtained by D19 and the uncertainty of each value is also included here.

The values of F listed in Tables 1 and 2 were substituted into eqs. (9-12) to solve for $(M_{\text{dyn}}/M_{\text{irr}})$, $(M_{\text{spin}}/M_{\text{dyn}})$, $(M_{\text{spin}}/M_{\text{irr}})$ and $(E_{\text{spin}}/E_{\text{spin,max}})$, and the results are listed in Tables 1 and 2 and illustrated in Figures 7 - 14. Uncertainties of these quantities are obtained using the expressions listed at the end of section 2.2. Black hole masses obtained from McLure et al. (2004, 2006) and listed by D19 were applied using eq. (13) to obtain M_{spin} ; the results are illustrated in Figs. 15 and 16 and listed in the Tables. The total outflow energy, E_{T} , was obtained as described by O’Dea et al. (2009) (see also Leahy et al. 1989; Daly 2002), and the values relative to the spin energy available for extraction, $(E_{\text{T}}/E_{\text{spin}})$, and relative to the black hole dynamical mass, $(E_{\text{T}}/M_{\text{dyn}})$, are listed in the Tables and illustrated in Figs. (17-20). Uncertainties for all quantities were obtained by propagating through from the original uncertainties on all quantities. In all of the histograms, the bin size was selected to be similar to the mean uncertainty of the quantity presented. It is helpful to consider the redshift distribution of each quantity when viewing the histograms to get some perspective on the contributions to the histograms from sources at different redshift. For many quantities of interest, sources with low values drop out as the redshift increases, which causes the low end of the histogram to be depleted of similar sources that are likely to exist at higher redshift. This can be explained by the fact that the parent population of sources is derived from a flux limited sample, as discussed for example in section 2.3.

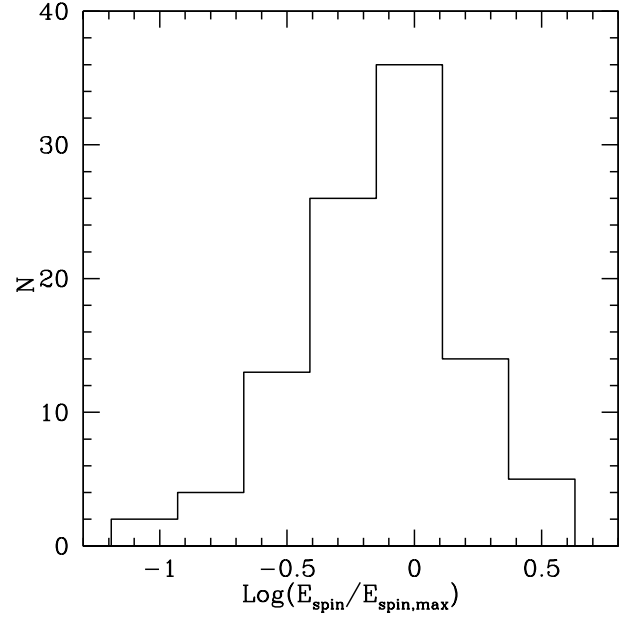


Figure 7. Histogram of $\text{Log}(E_{\text{spin}}/E_{\text{spin,max}})$. A value of $F = 1$ (i.e. $\text{Log}(F) = 0$) substituted into eq. (12) indicates an expected maximum value of this quantity of 0. The sources with values greater than about zero are the sources with values of $\text{Log}(F) > 0$. For more information, see the caption to Fig. 5.

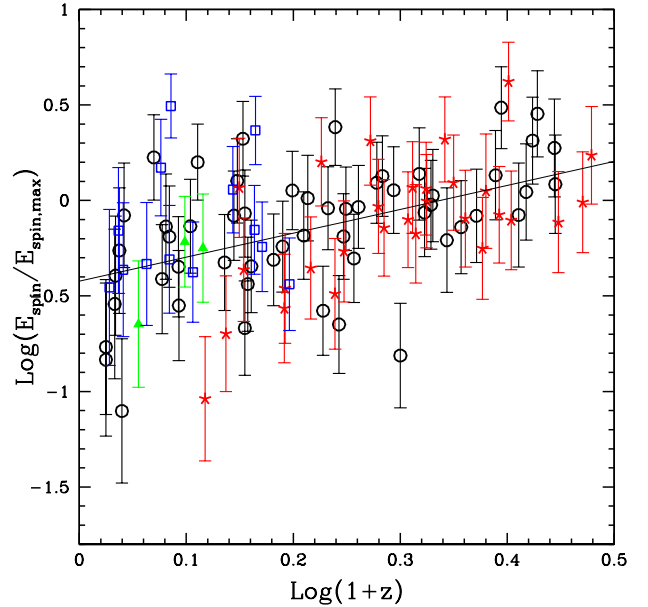


Figure 8. The redshift distribution of $\text{Log}(E_{\text{spin}}/E_{\text{spin,max}})$. A value of $F = 1$ or $\text{Log}(F) = 0$ indicates a value of $\text{Log}(E_{\text{spin}}/E_{\text{spin,max}})$ of zero. The symbols are as in Fig. 6 and the fit is unweighted. Values describing the best fit line can be deduced from those listed for $\text{Log}(M_{\text{spin}}/M_{\text{irr}})$ in Table 3, as described in the footnote to that Table.

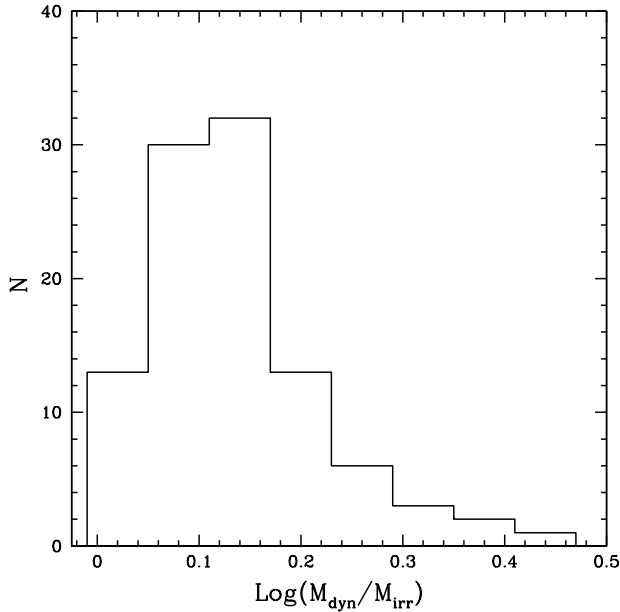


Figure 9. Histogram of $\text{Log}(M_{\text{dyn}}/M_{\text{irr}})$. A value of $F = 1$ substituted into eq. (9) indicates an expected maximum value of this quantity of about 0.15. The sources with values greater than about 0.15 are the sources with values of $\text{Log}(F) > 0$; almost all of these sources have uncertainties $\delta\text{Log}(M_{\text{dyn}}/M_{\text{irr}})$ that are within one to two sigma of 0.15. The same is true for all of the histograms that follow. For more information, see the caption to Fig. 5.

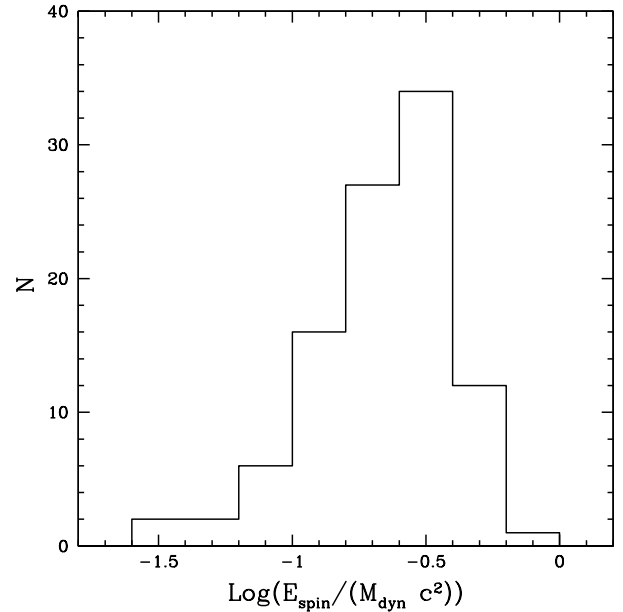


Figure 11. Histogram of $\text{Log}(E_{\text{spin}}/(M_{\text{dyn}} c^2))$, or $\text{Log}(M_{\text{spin}}/M_{\text{dyn}})$. A value of $F = 1$ substituted into eq. (11) indicates an expected maximum value of this quantity of about -0.53. For more information, see the caption to Fig. 5.

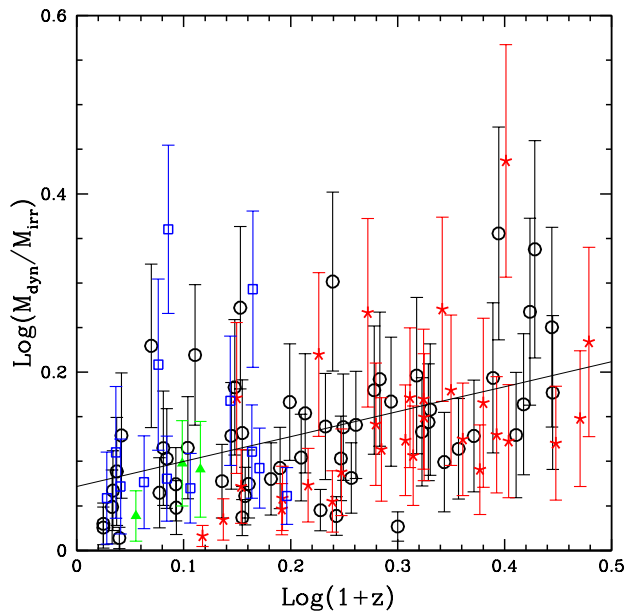


Figure 10. The redshift distribution of $\text{Log}(M_{\text{dyn}}/M_{\text{irr}})$. A value of $F = 1$ indicates a value of $\text{Log}(M_{\text{dyn}}/M_{\text{irr}})$ of about 0.15. The symbols are as in Fig. 6 and the fit is unweighted.

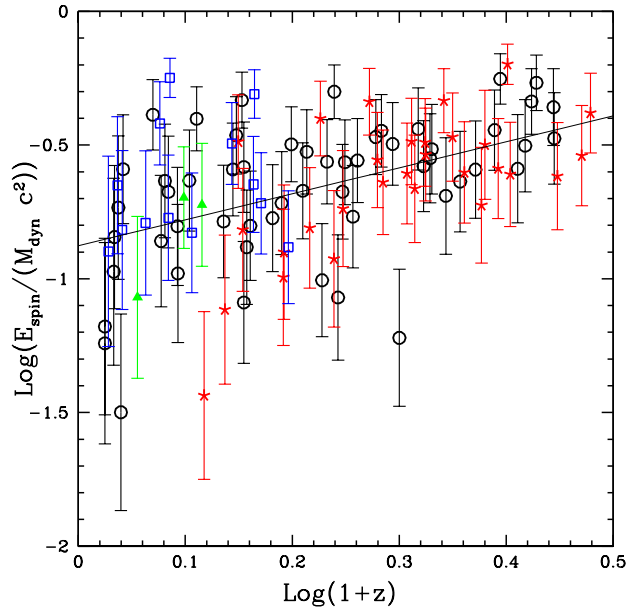


Figure 12. The redshift distribution of $\text{Log}(E_{\text{spin}}/(M_{\text{dyn}} c^2))$, or $\text{Log}(M_{\text{spin}}/M_{\text{dyn}})$. The theoretically expected maximum value of this quantity is about -0.53. Symbols and information are as in Fig. 6.

4 DISCUSSION

4.1 Characteristics that Depend only upon the Spin Function

The properties of the spin function are described in section 2.3. The properties of the quantities obtained with the spin function reflect the properties of the spin function.

The fraction of the total dynamical black hole mass, M_{dyn}

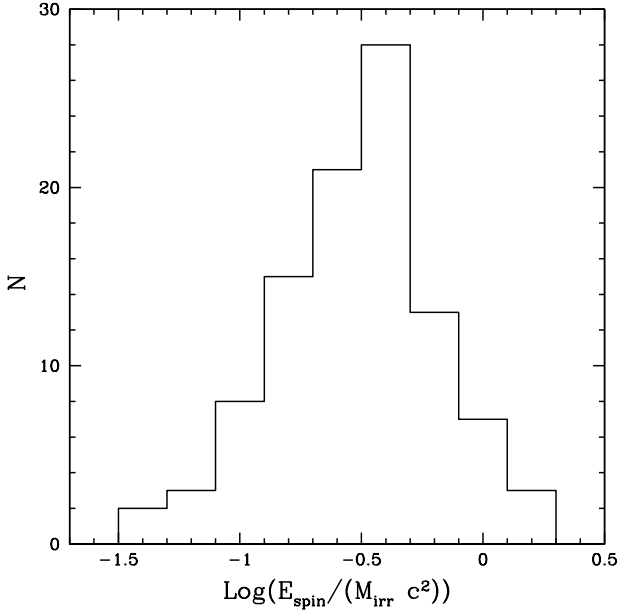


Figure 13. Histogram of $\text{Log}(E_{\text{spin}}/(M_{\text{irr}}c^2))$, or $\text{Log}(M_{\text{spin}}/M_{\text{irr}})$. A value of $F = 1$ substituted into eq. (11) indicates an expected maximum value of this quantity of about -0.38 . For more information, see the caption to Fig. 5.

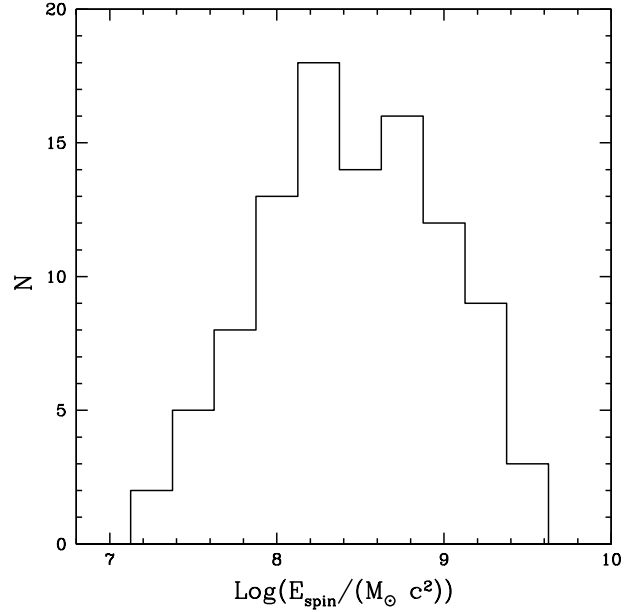


Figure 15. Histogram of $\text{Log}(E_{\text{spin}}/(M_{\odot}c^2))$, or $\text{Log}(M_{\text{spin}}/M_{\odot})$ obtained with eq. (13). For more information, see the caption to Fig. 5.

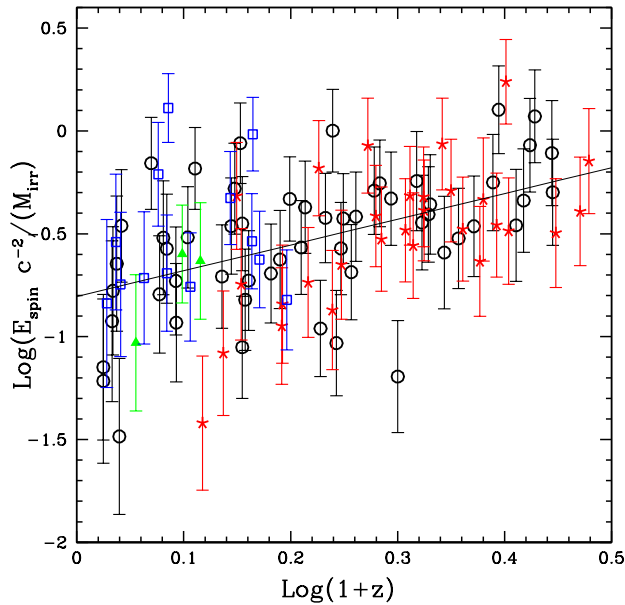


Figure 14. The redshift distribution of $\text{Log}(E_{\text{spin}}/(M_{\text{irr}}c^2))$, or $\text{Log}(M_{\text{spin}}/M_{\text{irr}})$. The theoretically expected maximum value of this quantity is about -0.38 . Symbols and information are as in Fig. 6.

that is associated with the black hole spin mass-energy, $M_{\text{spin}} = E_{\text{spin}}/c^2$, typically is close to the maximum possible value for the classical double radio sources studied here. For example, the mean values of HEG, Q, and LEG sources for the quantities $\text{Log}(M_{\text{dyn}}/M_{\text{irr}})$, $\text{Log}(M_{\text{spin}}/M_{\text{dyn}})$, $\text{Log}(M_{\text{spin}}/M_{\text{irr}})$, $\text{Log}(F)$, and $\text{Log}(E_{\text{spin}}/E_{\text{spin,max}})$ are less than though close to the predicted maximum values of these quantities of about 0.15 , -0.53 , -0.38 , 0 , and 0 , respectively (see Table 3). The W sources, which are all low

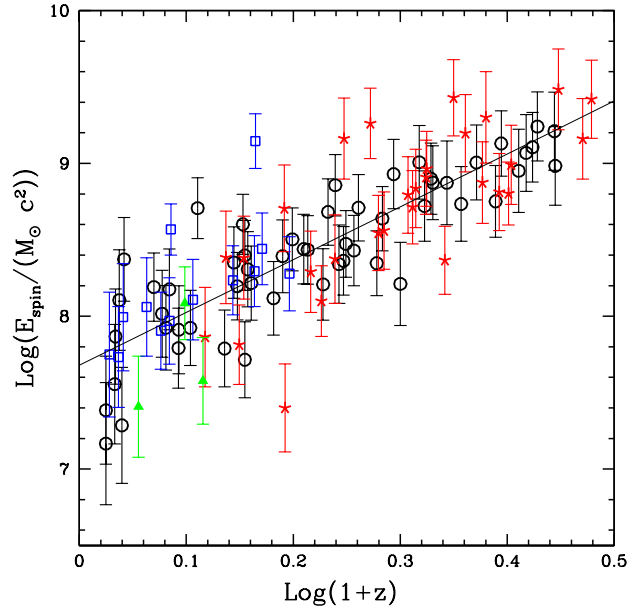


Figure 16. The redshift distribution of $\text{Log}(E_{\text{spin}}/(M_{\odot}c^2))$, or $\text{Log}(M_{\text{spin}}/M_{\odot})$ obtained with eq. (13). Symbols and information are as in Fig. 6.

redshift sources, have smaller mean values of all of these quantities relative to the other source types (and all of their values are close to the y-intercept values). This is not surprising since these quantities shown as a function of redshift clearly illustrate that sources with lower values of these quantities drop out as redshift increases due to well known selection effects. The classical double sources studied have redshifts between about zero and 2, and are selected from the 178 MHz radio flux limited 3CRR sample, described by Laing, Riley, & Longair (1983), as discussed in section 2.3. It is easy to

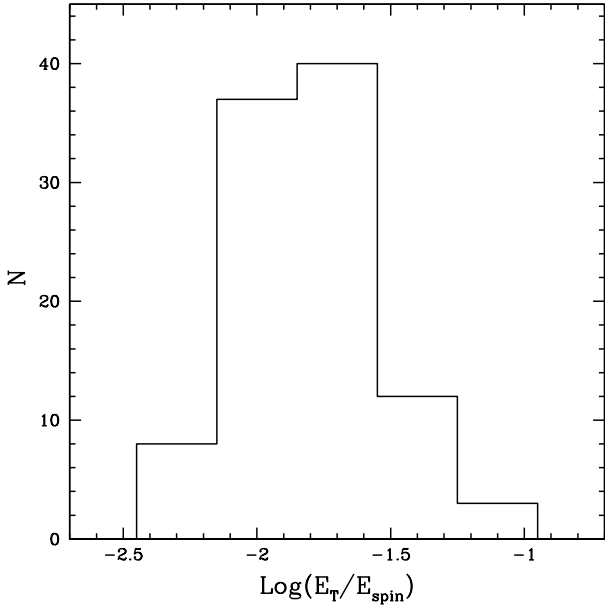


Figure 17. Histogram of the Log of the total energy output by the dual collimated jets during the outflow event, E_T , relative to the black hole spin energy available, E_{spin} . The theoretically expected maximum value of this quantity is 0. For more information, see the caption to Fig. 5.

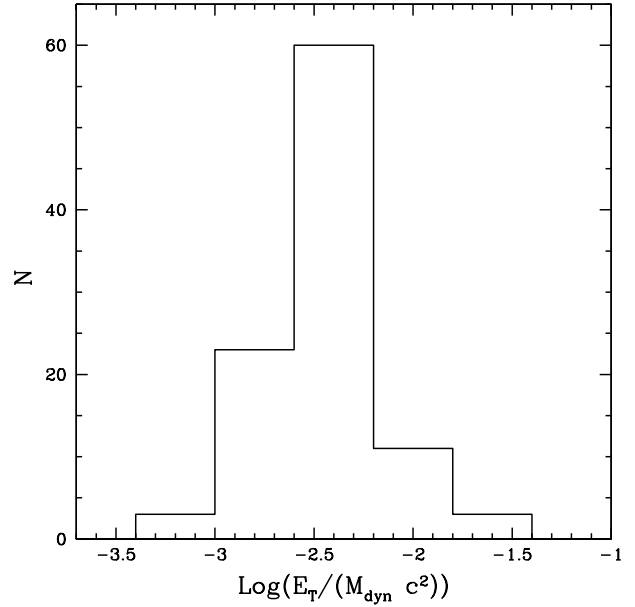


Figure 19. Histogram of the Log of the total energy output in the form of dual collimated jets during the outflow event, E_T , relative to the total (dynamical) black hole mass, M_{dyn} . For more information, see the caption to Fig. 5.

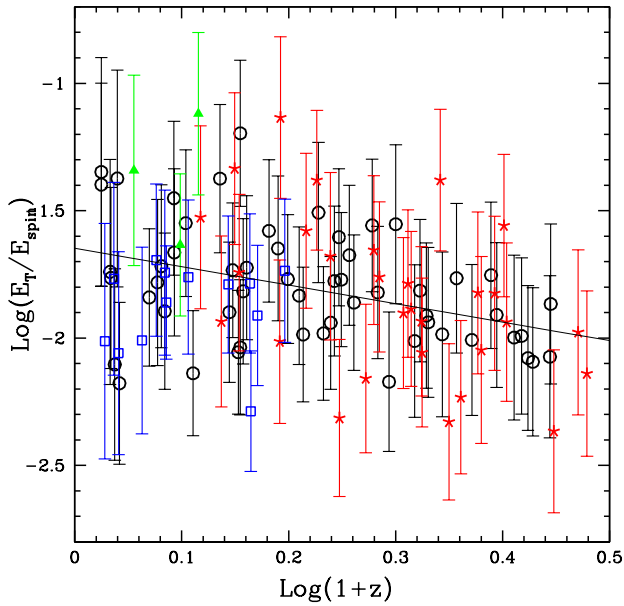


Figure 18. Log of the total energy output in the form of dual collimated jets during the outflow event, E_T , relative to the spin energy available, E_{spin} , vs $\text{Log}(1+z)$. The theoretically expected maximum value of this quantity is 0. Symbols and information are as in Fig. 6.

see the impact of missing lower luminosity sources as redshift increases. Note that the upper envelope of the distributions provides a guide as to how parameters that describe sources with the largest spin functions, which are typically sources with the highest beam powers relative to the Eddington luminosity, evolve with redshift.

The fact that black holes associated with the production of the

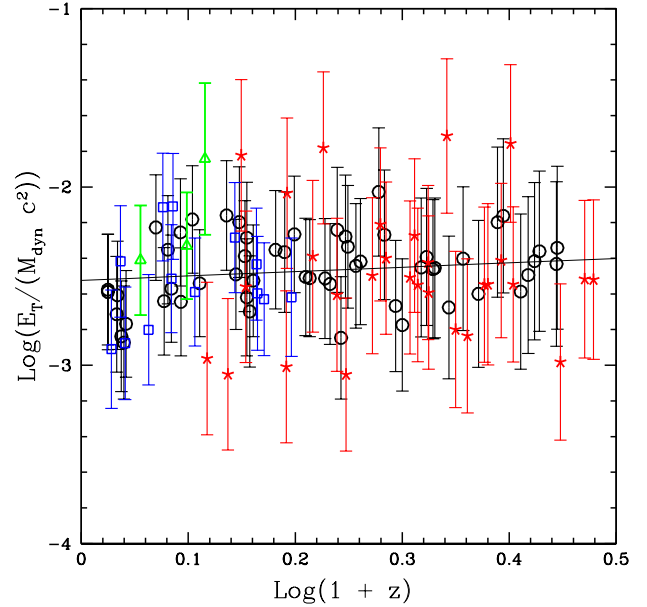


Figure 20. Log of the total energy output in the form of dual collimated jets during the outflow event, E_T , relative to total dynamical black hole mass, M_{dyn} , vs $\text{Log}(1+z)$. Symbols and information are as in Fig. 6.

classical double radio sources studied here have values of F close to unity and thus are very rapidly spinning is not surprising. Given that classical double radio sources are among the most powerful long-lived outflows observed in the universe, it is expected that they would be produced by rapidly spinning black holes with spin energies close to the maximum possible value (e.g. Rees 1984; Begelman, Blandford, & Rees 1984; Blandford 1990).

The values of $\text{Log}(E_{\text{spin}}/E_{\text{spin,max}})$, $\text{Log}(M_{\text{dyn}}/M_{\text{irr}})$, $\text{Log}(M_{\text{spin}}/M_{\text{dyn}})$, and $\text{Log}(M_{\text{spin}}/M_{\text{irr}})$ are listed in Tables 1 and 2 are consistent with or less than the maximum expected values about 0, 0.15, -0.53, and -0.38 within one to two sigma, and have distributions that reflect those of the spin functions used to obtain these values.

Equation (14) indicates that the rotational mass defined in section 1 relative to the irreducible mass is equal to F , the square root of the spin function. This means that the distribution of values of $\text{Log}(M_{\text{rot}}/M_{\text{irr}})$ is the same as that discussed for $\text{Log}(F)$ in section 2.3 for the 100 supermassive black holes studied here. Thus, about 2/3 (or about 66) of the 100 sources studied here have a Gaussian distribution of $\text{Log}(M_{\text{rot}}/M_{\text{irr}})$ with a mean value of zero and standard deviation of about 0.15. The remaining 1/3 (or about 34 sources) have $\text{Log}(M_{\text{rot}}/M_{\text{irr}}) < 0$, with the tilted distribution described in section 2.3. This also means that the values of $\text{Log}(F)$ obtained by D19 for black holes associated with 656 additional AGN and 102 measurements of four stellar mass black holes translate directly to empirically determined values of $\text{Log}(M_{\text{rot}}/M_{\text{irr}})$. Finally, eq. (15) indicates that values of $\text{Log}(M_{\text{rot}}/M_{\text{dyn}})$ can also be obtained for the 100 sources studied here plus the additional AGN and stellar mass black holes mentioned above.

4.2 Spin Mass-Energy

The spin mass-energy per source available for extraction is obtained using eq. (13) where $M = M_{\text{dyn}}$ is the empirically determined dynamical mass of the black hole. The black hole masses listed in D16 and D19 are applied here, and were obtained from McLure et al. (2004, 2006). In computing the uncertainty of the spin mass-energy that is listed in the Tables, the way that the empirically determined black hole mass enters into the empirically determined black hole spin function $F \propto M_{\text{dyn}}^{-0.28}$ (e.g. D19) is taken into account.

The spin mass-energy associated with black holes is an energy reservoir that is available to be tapped and when tapped can significantly affect the black hole environment; this is referred to as the "spin energy reservoir." For supermassive black holes, this can significantly affect the host galaxy and the environment in the vicinity of the host galaxy, as discussed in section 1 (see also Donahue & Voit 2022 and references therein).

As indicated in Figs. 15 and 16, the energy that is available per black hole is quite substantial. Since the black hole mass associated with classical double radio sources is strongly evolving with redshift, so is the spin mass-energy (see eq. 13). It is clear that sources at lower redshift contribute to the low mass end of the histogram while sources at higher redshift contribute to the high mass end of the histogram. The spectroscopic types that contribute to the lower spin energy end of the histogram include LEG and W sources, which are prevalent at lower redshift, while Q sources are prevalent at higher redshift and contribute preferentially to the high spin energy end of the histogram. The HEG sources contribute at all redshifts, as is evident from Fig. 16.

4.3 Total Outflow Energy Relative to Spin Mass-Energy and Relative to Dynamical Black Hole Mass

The fraction of the available spin energy that is produced per outflow event, $(E_{\text{T}}/E_{\text{spin}})$, is obtained by dividing the total energy that is carried away from the black hole system during the outflow event, E_{T} , by the spin energy that is available, E_{spin} . And, the total outflow energy relative to the total (dynamical) black hole mass

is $(E_{\text{T}}/M_{\text{dyn}})$. Note that the empirically determined quantities E_{T} and M_{dyn} are obtained with completely independent methods. The range of values for the total outflow energy per source, E_{T} , span about an order of magnitude (e.g. see Figs. 40 and 41 from O'Dea et al. 2009), the range of values of E_{spin} span about two orders of magnitude (see Figs. 15 and 16), and the range of values of values of M_{dyn} span about two orders of magnitude (see Fig. 3 of D19).

The total outflow energy is obtained by multiplying the total outflow timescale by the beam power, where the beam power is the energy per unit time output in the form of dual jets from the black hole system (e.g. O'Dea et al. 2009). It has been shown conclusively for classical double (FR II) sources such as those studied here that the total outflow timescale is very well characterized as a function of only the beam power (Daly 1994; Daly et al. 2008, 2009). Note that the relationship between the total outflow timescale and the beam power is the foundation of the use of classical double radio galaxies for cosmological studies. The fact that this application for cosmological studies yields results that are very similar to and consistent with those obtained with other methods indicates that this model is on secure footing, as discussed in detail, for example, by Daly et al. (2008, 2009).

The total outflow energy per source obtained by O'Dea et al. (2009) is used here, and an identical method is applied to obtain the total outflow lifetime from the beam power and thus the total outflow energy for the remaining sources in the sample. The total outflow energy per source, referred to as E_{T} , is divided by the spin energy E_{spin} to obtain the fraction of the spin energy that could be extracted per outflow event, $(E_{\text{T}}/E_{\text{spin}})$. And, E_{T} is divided by the black hole mass M_{dyn} to obtain the fraction of the black hole mass that is produced per outflow event, $(E_{\text{T}}/M_{\text{dyn}})$. Note that the total outflow energy E_{T} is independent of the black hole mass and only depends on the beam power of the source, which is empirically determined using the strong shock method (reviewed in detail by O'Dea et al. 2009).

The results obtained here indicate that only a small fraction, about 1.5% of the spin energy available per black hole is produced per outflow event; see the values listed in Tables 1 and 2, and summarized in Table 3. The fraction $(E_{\text{T}}/E_{\text{spin}})$ is independent of source type (see Table 3), except for the W sources, and there are only three low redshift W sources in the sample. The results indicate that the mean value of $\text{Log}(E_{\text{T}}/E_{\text{spin}})$ for the 100 sources studied is about $\text{Log}(E_{\text{T}}/E_{\text{spin}}) \approx -1.81 \pm 0.26$. This translates to a small fraction of the black hole dynamical mass being output per outflow event, as indicated by the values of $\text{Log}(E_{\text{T}}/M_{\text{dyn}})$ listed in Tables 1 and 2 and summarized in Table 3. The mean value of this quantity is $\text{Log}(E_{\text{T}}/M_{\text{dyn}}) \approx -2.47 \pm 0.27$ for the 100 sources studied. This translates to a mean value of the total outflow energy relative to dynamical black hole mass of about $(E_{\text{T}}/M_{\text{dyn}}) \approx 3.4 \times 10^{-3}$. These results are consistent with those obtained by Daly (2009a) who studied a sample of 19 classical double radio sources and found that about a few $\times 10^{-3}$ of the black hole dynamical mass is output in the form of large-scale jets per source per outflow event. As mentioned earlier, there is no overlap in the methods used to obtain E_{T} and M_{dyn} .

There are several possible explanations for the fact that the total energy output over the source lifetime in the form of large-scale jets is small compared with the black hole dynamical mass and compared with the spin energy available for extraction, and that each has a relatively narrow distribution. 1. When a certain fraction of the black hole mass-energy is deposited into the ambient gas, the gas is heated and expands, and the accretion is shut off; this would be consistent with the result obtained here and by Daly

(2009a). 2. The spin energy extraction, which decreases the black hole dynamical mass, destabilizes the black hole - accretion disk - magnetic field configuration causing the spin energy extraction to be terminated. 3. The black hole masses have been overestimated, and the total spin energy available for extraction is smaller than obtained based on current black hole mass estimates; this would increase the ratio (E_T/E_{spin}) and the ratio (E_T/M_{dyn}) . 4. The beam powers are much much larger than indicated empirically, and thus carry away significantly more energy than already accounted for. 5. The black hole spin function F , and thus dimensionless spin angular momentum and spin energy, has been overestimated. This would only impact E_{spin} and thus (E_T/E_{spin}) , but would not impact M_{dyn} and thus would not impact (E_T/M_{dyn}) . 6. Only transitions between particular spin states are allowed, as described by Pugliese & Quevedo (2022) and Pugliese & Stuchlík (2021). 7. Something else. Each of these possibilities is considered.

Possibility 1. could explain the observed values and small range of values of the quantities (E_T/E_{spin}) and (E_T/M_{dyn}) obtained here and by Daly (2009a). The results indicate that the energy deposited into the ambient gas over the entire lifetime of an FR II source relative to the black hole dynamical mass is about $\text{Log}(E_T/M_{\text{dyn}}) \simeq (-2.47 \pm 0.27)$ (see Table 3 and Fig. 19 in this work, and Table 1 and Fig. 1 from Daly 2009a). These results are consistent with the empirically determined value of about -2.3 ± 0.5 obtained by Donahue & Voit (2022) (see their Fig. 20) based on empirical studies of the energy input required to heat and lift the circumgalactic medium and shut off accretion for a sample of relatively low redshift sources. One interesting caveat is that the FR II sources studied here have redshifts between about zero and two, and the source sizes change significantly with redshift (e.g. Fig. 8 of Guerra, Daly, & Wan 2000), so the result obtained here would have to be independent of the details of the energy input such as where in the galactic and circumgalactic medium the energy is deposited and independent of the structure (density and temperature) of the galactic and circumgalactic medium.

In this scenario, the accretion would be shut off by the heating and lifting of the circumgalactic medium; the medium would eventually settle down and another outflow episode would occur. Each outflow event would decrease the black hole spin energy by a very small amount, as long as the angular momentum extracted during the outflow event exceeds that gained by the black hole during the accretion event. One puzzling factor for this interpretation is that the range of values of (E_T/M_{dyn}) and (E_T/E_{spin}) obtained here and by Daly (2009a) are narrow, and seemingly independent of radio source size and source redshift (see Fig. 20, and the value of the slope listed in Table 3).

One rather radical idea to explain the small values and small range of these quantities is to posit that the majority of the spin energy is extracted per outflow event, but most of it does not end up in the form of a dual collimated outflow (which would comprise a set fraction of the total energy extracted per unit time), but is in some difficult to detect form such as neutrinos, or gravitational waves. In the outflow method, the normalization of eq. (1) is a free parameter that is empirically determined. The empirically determined value is consistent with the theoretical prediction in the Meier (1999) model (see section 3.3 of D19), and is also consistent with the normalization in the Blandford & Znajek (1977) model.

Thus, this hypothetical other process would occur simultaneously with the Blandford & Znajek (1977) or Meier (1999) mechanism but would extract substantially more spin energy per unit time, by factors of about (10 - 100), and the energy extracted would be in

some form that is not readily observable. This process could work hand-in-hand with possibilities 2 and/or 3.

Note that for FR II sources the outflow timescale depends only upon the beam power, indicating that the accretion timescale must exceed the outflow timescale unless some process directly related to the beam power shuts off the accretion. Otherwise, the outflow timescale would be set by the accretion timescale and would not be a function of only the beam power, as has been shown conclusively by Daly et al. (2009).

Possibility 2. is quite interesting. As the spin energy is extracted, the black hole mass decreases causing the accretion disk to expand slightly and over a long period of time; the outflow timescales are typically a few $\times 10^7$ years (e.g. O’Dea et al. 2009). If the stability of the magnetic field that plays a crucial role in the spin energy extraction requires a particular ratio of the disk thickness to the disk radius, as the disk expands the thin disk may be disrupted. That is, it is possible that the disk and thus the anchor of the magnetic field is disrupted when the fraction of the black hole dynamical mass is decreased by the particular value of a few tenths of a percent found here and by Daly (2009a). The decrease of the black hole mass would have a small impact on the radius of the disk, but could have a large impact on the disk thickness, which is likely to be small relative to the disk radius (see, for example, Blandford & Globus 2022; Kolos et al. 2021). Possibility 2. could work hand-in-hand with possibility 1. It’s not clear how large a fraction of the black hole mass-energy would have to be removed to de-stabilize the accretion disk - magnetic field - black hole configuration and thus terminate the outflow. This possibility would be more palatable if the fraction of the black hole mass removed was larger, as considered in point 3.

This brings us to possibility 3. If the black hole masses have been systematically overestimated, then the spin energy values obtained with eq. (13) decrease and the ratios (E_T/E_{spin}) and (E_T/M_{dyn}) increase. There are some recent studies that suggest that black hole dynamical masses may be systematically overestimated (e.g. Grier et al. 2019). However, the brightest sources studied here and by D19 have a bolometric accretion disk luminosity that is right at the Eddington luminosity (see Fig. 4 of D19), and any decrease in black hole mass would cause these sources to be radiating at super-Eddington levels.

Possibility 4 is very unlikely based on the following. The direct comparison between the total outflow energy and the black hole mass indicates that the outflow energy is a roughly constant fraction of the black hole mass, with $(E_T/M_{\text{dyn}}) \approx 3 \times 10^{-3}$ independent of the spin properties of the black hole (see Figs. 19 and 20, Tables 1, 2, and 3, and Daly 2009a). As noted by O’Dea et al. (2009), the total outflow energy scales as the beam power $L_j^{0.5}$, so to significantly increase the outflow energy by factors of 10 to 100, the beam power would have to increase by factors of $10^2 - 10^4$, which is highly unlikely since the beam power is insensitive to offsets from minimum energy conditions (e.g. O’Dea et al. 2009). In addition, the largest beam powers are about 10 % of the Eddington luminosity (e.g. Daly et al. 2018), so this would require the maximum beam powers to be significantly larger than the Eddington luminosity. And, as noted above, the empirically determined beam power normalizations match those predicted theoretically in the Meier (1999) and Blandford & Znajek (1977) models.

Possibility 5. is unlikely because independent spin determinations for supermassive black holes associated with classical double radio sources agree with those obtained with the outflow method, and indicate high spin values (e.g. Azadi et al. 2020). Fifteen of the quasars studied by D19 with the outflow method overlap with

those studied by Azadi et al. (2020) with the continuum fitting method, and the spin values obtained with the independent methods agree. Similarly, for local AGN, spin values obtained with the outflow method agree with those obtained independently with the X-ray reflection method for the six sources for which a comparison was possible (D19). Possibility 5. would require that spin determinations published to date for supermassive black holes by other groups using independent methods are incorrect by large factors.

Other options are possibility 6., only transitions between particular black hole spin states are allowed as described by Pugliese & Quevedo (2022) and Pugliese & Stuchlík (2021), or possibility 7, something else.

5 SUMMARY

Mass-energy characteristics of black holes are obtained in terms of the black hole spin function, F^2 . Empirically determined black hole spin functions are used to obtain and study the spin mass-energy properties of a sample of 100 supermassive black holes associated with classical double (FR II) radio sources with dual collimated outflows; the sources have redshifts between about zero and two. Black hole spin mass-energy that is available to be extracted from the black hole is $M_{\text{spin}} = M - M_{\text{irr}}$, where $M \equiv M_{\text{dyn}}$ (see eq. 2). The mass-energy associated with the black hole spin angular momentum J , referred to here as M_{rot} and defined in section 1, contributes to the total black hole mass, M : $M^2 = M_{\text{irr}}^2 + M_{\text{rot}}^2$, which leads to eqs. (3) and (9). These equations are combined to obtain expressions that describe black hole spin mass-energy characteristics in terms of the spin function, which are then applied to quantify and study empirically determined black hole spin mass-energy properties for a sample of 100 supermassive black holes. It is important to be able to empirically determine black hole spin mass-energy characteristics because these impact the total black hole mass, and because this energy can be extracted, which may impact the near and far field environments of astrophysical black holes.

The relationship between the beam power in Eddington units and bolometric accretion disk luminosity in Eddington units for the sample of supermassive black holes studied here is very similar to and consistent with that obtained for three other samples of sources with very different ranges and values of Eddington normalized beam power and bolometric disk luminosity (Daly et al. 2018). The samples studied include the 100 sources studied here plus 656 AGN and 102 measurements of four stellar-mass black holes that are in X-ray binary systems, and include several different types of AGN. This suggests that the outflows in all of these systems are produced by a common physical mechanism. Since many of the sources studied by Daly et al. (2018) have beam powers that are much larger (by factors of 10 to 100) than the bolometric accretion disk luminosity, these sources are likely to have spin-powered outflows. Since the outflows in all of the sources studied are likely to be produced by a common physical mechanism, this suggests that all of the sources, including those studied here, have spin powered outflows.

Quantities that characterize the spin mass-energy properties of astrophysical black holes in terms of the black hole spin function, F^2 , are presented in section 2.2. This is preferable for astrophysical black holes for several reasons. For example, when attempting to use the dimensionless black hole spin angular momentum $j \equiv Jc/(GM^2)$ to empirically characterize and determine the spin properties of astrophysical black holes, several difficulties are encountered, as described in section 2.1. These issues may be avoided and circumvented by writing the black hole spin mass-energy char-

acteristics in terms of the black hole spin function F^2 . Furthermore, in the context of the outflow method, the empirically determined quantity is F .

Relationships between the black hole spin mass-energy characteristics and the black hole spin function F^2 are obtained and presented in section 2.2. It is found that there is roughly a linear relationship between the black hole spin function and the normalized spin mass-energy of the black hole ($E_{\text{spin}}/E_{\text{spin,max}} \approx F^2$), and allowing the exponent of F to vary, that $\text{Log}(E_{\text{spin}}/E_{\text{spin,max}}) \approx 1.75 \text{Log}(F)$ over the range of values relevant to the current studies. In addition, the method allows for empirically determined values of the spin function that exceed unity, which can occur due to the uncertainties associated with empirically determined quantities for astrophysical black holes.

The method described in section 2.2 is applied to a sample of 100 supermassive black holes with redshifts between about zero and 2. The values of $\text{Log}(F)$ studied here were obtained by D19, and are listed along with their uncertainties in Tables 1 and 2. It is shown in section 2.3 that the sample is well represented as having two components: about 2/3 of the 100 sources are maximally spinning, and about 1/3 are less than maximally spinning with the number of sources per unit $\text{Log}(F)$ declining as $\text{Log}(F)$ decreases. The decreasing number of sources as $\text{Log}(F)$ decreases could be due to observational selection effects, a real decline with $\text{Log}(F)$, or a combination of the two. The 100 FR II sources studied include four sub-samples based on their spectroscopic nuclear properties; HEG, LEG, Q, and W sources, as described in section 2.3. As is evident from Table 3, the results presented here are, for the most part, independent of source spectroscopic nuclear properties, except for the W sources, and there are only three low-redshift W sources in the sample.

Interestingly, it turns out that $\text{Log}(M_{\text{rot}}/M_{\text{irr}}) = \text{Log}(F)$ (see eq. 14), so all of the comments and results obtained for $\text{Log}(F)$ directly apply to $\text{Log}(M_{\text{rot}}/M_{\text{irr}})$. Thus, the distribution of values of $\text{Log}(F)$ described in section 2.3 can be interpreted as the empirically determined distribution of values of $\text{Log}(M_{\text{rot}}/M_{\text{irr}})$. The empirically determined values of $\text{Log}(F)$ and their uncertainties for an additional 656 AGN and 102 measurements of four stellar mass black holes listed and discussed by D19 also directly translate to values of $\text{Log}(M_{\text{rot}}/M_{\text{irr}})$ for those sources. The quantity $\text{Log}(M_{\text{rot}}/M_{\text{dyn}})$ can be obtained from eq. (15), which indicates that $\text{Log}(M_{\text{rot}}/M_{\text{dyn}}) = \text{Log}(F) - \text{Log}(M_{\text{dyn}}/M_{\text{irr}})$, both of which are listed in Tables 1 and 2.

Results describing the spin mass-energy characteristics of the 100 sources are presented and discussed in sections 3 and 4. Many of the sources are highly spinning, and the sources with lower values of black hole spin are at low redshift, as expected due to the flux limited nature of the parent population of the sources. Thus, the fact that many of the sources are highly spinning may be a selection effect in that the most highly spinning sources have the brightest and most powerful radio emission, and less powerful sources drop out of the sample at high redshift due to the flux limited nature of the parent population, as described in sec. 2.3.

The spin mass-energy values obtained from the black hole spin functions are studied relative to the total or dynamical black hole mass and relative to the irreducible black hole mass. For maximally spinning black holes, the mass-energy associated with the black hole spin contributes about 41 % relative to the irreducible black hole mass or about 29 % relative to the total dynamical black hole mass. This mass-energy can be extracted (Penrose 1969). Thus, the mass of the black hole can be decreased due to the extraction of the spin energy. In addition, the extraction of the spin energy can

significantly affect the short and long range environment of each black hole. Since these are all FR II (classical double) radio sources, these sources channel energy significant distances (hundreds of kpc) from the supermassive black hole.

The spin mass-energy relative to the dynamical (i.e. total) black hole mass can be combined with empirical determinations of the black hole mass to solve for the total spin energy available for extraction per source, as discussed in detail in sections 1 and 2 (see eq. 13). The spin energy per supermassive black hole is substantial, and represents an important reservoir of energy that can be tapped; this is referred to as the "spin energy reservoir." Tapping even small amounts of the spin energy can have a substantial impact on the near and far field environments of the sources, as discussed in sections 4.2 and 4.3.

The total spin energy available per source is compared with the total energy output from the black hole system in the form of dual oppositely directed jets over the active lifetime of each source, E_T , as described in sections 3 and 4.3. For the 100 black hole systems studied, the range of values of (E_T/E_{spin}) , the ratio of the total outflow energy to the spin energy available, is very narrow, with most of the sources having a value of about one percent or so: $\text{Log}(E_T/E_{\text{spin}}) \approx -1.8 \pm 0.3$ for the 100 FR II sources studied here. This is consistent with the results obtained here and by Daly (2009a) that indicated a small value and range of values of total outflow energy relative to black hole dynamical mass: $\text{Log}(E_T/M_{\text{dyn}}) \approx -2.5 \pm 0.3$ for the 100 FR II sources studied here (see sections 3 and 4.3). The value obtained here is consistent with that obtained by Daly (2009a) and that with obtained with a different method applied to different types of sources by Donahue & Voit (2022), who find $\text{Log}(E_T/M_{\text{dyn}}) \approx -2.3 \pm 0.5$ for a sample of low redshift sources. The small value and restricted range of values of $\text{Log}(E_T/M_{\text{dyn}})$ could suggest that this is a fundamental property of the primary process responsible for producing the dual collimated outflows.

Several possible explanations for the relatively small value and range of values of (E_T/M_{dyn}) or (E_T/E_{spin}) are considered in section 4.3. For example, it could be that when a specific amount of energy relative to the dynamical black hole mass is dumped into the ambient medium, the ambient gas is heated and expands, shutting off the accretion. Another possibility is that as the spin energy is extracted and the black hole mass decreases, the magnetic field and/or the structure of the accretion disk is altered and the spin energy extraction is halted. Or, it could be that much of the spin energy is extracted and then the process shuts down - if the black hole masses have been systematically overestimated, then the black hole mass that enters into eq. (13) is decreased and the spin energies decrease, so a correspondingly larger fraction of the spin energy is extracted per outflow event. Another possibility discussed in section 4.3 is that there is some other process that occurs simultaneously with the process that leads to dual large-scale jets, and this other process is extracting the majority of the spin energy, but the extracted energy is released in a form that is not readily observable. For example, most of the spin energy could be carried away in the form of neutrinos or gravitational waves, and only a small fraction of the energy extracted would be channeled into the jetted dual outflow.

The new method of obtaining black hole spin mass-energy characteristics directly from the spin function presented here is applicable to the study of astrophysical black holes in a broad range of contexts.

ACKNOWLEDGMENTS

Thanks are extended to the referee, Kastytis Zubovas, for a careful reading of the manuscript and for providing very helpful comments and suggestions. It is a pleasure to thank Megan Donahue, Jim Pringle, and Mark Voit for detailed discussions and suggestions related to this work. I would also like to thank Jean Brodie, Margaret Daly, Joshua Deal, Yan-Fei Jiang, Chiara Mingarelli, Chris O'Dea, Masha Okounkova, Enrico Ramirez-Ruiz, Biny Sebastian, and Rosie Wyse for helpful conversations related to this work. It is a pleasure to thank the Center for Computational Astrophysics and the Flatiron Institute, which is supported by the Simons Foundation, for their hospitality. This work was performed in part at the Aspen Center for Physics, which is supported by National Science Foundation grant PHY-1607611.

6 DATA AVAILABILITY STATEMENT

The data underlying this article are available in the article or are listed in D19.

REFERENCES

- Azadi, M., Wilkes, B. Kuraszkiwicz, J., McDowell, J., Siebenmorgen, R., Ashby, M., Birkinshaw, M., Worrall, D., Abrams, N., Barthel, P., Fazio, G., Haas, M., Hyman, S., Martínez-Galarza, R., & Meyer, E., arXiv:2011.03130
- Antonini, F., Barausse, E., & Silk, J. 2015, *ApJ*, 806, L8
- Barausse, E., Shankar, F., Bernardi, M., Dubois, Y., & Sheth, R. K. 2017, *MNRAS*, 468, 4782
- Bardeen, J., Press, W., & Teukolsky, S. 1972, *ApJ*, 178, 347
- Beckwith K., Hawley J. F., Krolik J. H., 2008, *ApJ*, 678, 1180
- Begelman, M. C., Blandford, R. D., & Rees, M. J. 1984, *RvMp*, 56, 255
- Belsole, E., Worrall, D. M., Hardcastle, M. J., & Croston, J. H. 2007, *MNRAS*, 381, 1109
- Berti, E., Cardoso, V., & Starinets, A. O. 2009, *CQGrA*, 26, 163001
- Berti, E., & Volonteri, M. 2008, *ApJ*, 684, 822
- Blandford, R. D. 1990, in *Active Galactic Nuclei*, ed. T. J. L. Courvoisier & M. Mayor (Berlin: Springer), 161
- Blandford, R., & Globus, N. 2022, *MNRAS*, in press (arXiv:2204.11995)
- Blandford, R. D., & Znajek, R. L. 1977, *MNRAS*, 179, 433
- Brandt, W. N., & Alexander, D. M. 2015, *A&ARv*, 23, 1
- Bruni, G., Panessa, F., Bassani, L., Chiaraluca, E., Kraus, A., Dallacasa, D., Bazzano, A., Hernández-García, L., Malizia, A., Ubertini, P., Ursini, F., Venturi, T. 2019, *ApJ*, 875, 88
- Bruni, G., Panessa, F., Bassani, L., Dallacasa, D., Venturi, T., Saripalli, L., Brienza, M., Hernández-García, L., Chiaraluca, E., Ursini, F., Bazzano, A., Malizia, A., Ubertini, P. 2020, *MNRAS*, 494, 902
- Christodoulou, D. 1970, *Phys. Rev. Lett.* 25, 1596
- Daly, R. A. 1994, *ApJ*, 426, 38
- Daly, R. A. 1995, *ApJ*, 454, 580
- Daly, R. A. 2002, *NewAR*, 46, 47
- Daly, R. A. 2009a, *ApJL*, 691, L72
- Daly, R. A. 2009b, *ApJL*, 696, L32
- Daly, R. A. 2011, *MNRAS*, 414, 1253
- Daly, R. A. 2016, *MNRAS* 458, L24
- Daly, R. A. 2019, *ApJ*, 886, 37
- Daly, R. A. 2020, arXiv:2005.12201
- Daly, R. A., Djorgovski, S. G., Freeman, K. A., Mory, M. P., O’Dea, C. P., Kharb, P., & Baum, S. 2008, *ApJ*, 677, 1
- Daly, R. A., & Guerra, E. J. 2002, *ApJ*, 124, 1831
- Daly, R. A., Mory, M. P., O’Dea, C. P., Kharb, P., Baum, S., Guerra, E. J., Djorgovski, S. G. 2009, *ApJ*, 691, 1058
- Daly, R. A., & Sprinkle, T. B. 2014, *MNRAS* 438, 3233
- Daly, R. A., Stout, D. A., Mysliwiec, J. N. 2018, *ApJ*, 863, 117
- Davis, S. W., Laor, A., 2011, *ApJ*, 728, 98
- Dermer, C., Finke, J., & Menon, G. 2008, *Black-Hole Engine Kinematics, Flares from PKS2155-304, and Multiwavelength Blazar Analysis* (Trieste: SISSA)
- De Villiers J., Hawley J. F., Krolik J. H., 2003, *ApJ*, 599, 1238
- Donahue, M., & Voit, M. 2022, *PhR*, 973, 1
- Dubois, Y., Volonteri, M., & Silk, J. 2014, *MNRAS*, 440, 1590
- Fabian, A. C., Rees, M. J., Stella, L., & White, N. E. 1989, *MNRAS*, 238, 729
- Fanaroff, B. L., & Riley, J. M. 1974, *MNRAS*, 164, 31
- Ferrarese, L., Ford, H. 2005, *SSRv*, 116, 523
- Gammie, C. F., Shapiro, S. L., & McKinney, J. C. 2004, *ApJ*, 602, 312
- García, J. A., Steiner, J. F., McClintock, J. E., Remillard, R. A., Grinberg, V., & Dauser, T. 2015, *ApJ*, 813, 84
- Gardner E., Done C., 2018, *MNRAS*, 473, 2639
- Gerosa, D., Fabbri, C. M., & Sperhake, U. 2022, arXiv:2202.08848
- Ghisellini, G., Haardt, F., Della Ceca, R., Volonteri, M., & Sbarrato, T. 2013, *MNRAS*, 432, 2818
- Ghisellini G., Tavecchio F., Maraschi L., Celotti A., Sbarrato T., 2014, *Nature*, 515, 376
- Gnedin, Yu. N., Afanasiev, V. L., Borisov, N. V., Piotrovich, M. Yu., Natsvlshvili, T. M., & Buliga, S. D. 2012, *ARep*, 56, 573
- Grimes, J. A., Rawlings, S., & Willott, C. J. 2004, *MNRAS*, 349, 503
- Grier, C. J., Shen, Y., Horne, K., Brandt, W. N., Trump, J. R. et al. 2019, *ApJ*, 887, 38
- Guerra, E. J., Daly, R. A., & Wan, L. 2000, *ApJ*, 544, 659
- Hardcastle, M. J., & Croston, J. H. 2020, arXiv:2003.06137
- Hardcastle, M. J., Williams, W. L., Best, P. N., Croston, J. H., Duncan, K. J., Röttgering, H. J. A., Sabater, J., Shimwell, T. W., Tasse, C., Callingham, J. R., Cochrane, R. K., de Gasperin, F., Gürkan, G., Jarvis, M. J., Mahatma, V., Miley, G. K., Mingo, B., Mooney, S., Morabito, L. K., O’Sullivan, S. P. Prandoni, I., Shulevski, A., Smith, D. J. B. 2019, *A&A*, 622, A12
- Hughes, S. A., & Blandford, R. D. 2003, *ApJ*, 585, 101
- Iwasawa, K., Fabian, A. C., Reynolds, C. S., Nandra, K., Otani, C., Inoue, H., Hayashida, K., Brandt, W. N., Dotani, T., Kunieda, H., Matsuoka, M., & Tanaka, Y. 1997, in *Makino F., Mitsuda K., eds, X-Ray Imaging and Spectroscopy of Cosmic Hot Plasmas*. p. 247
- King, A. L., Miller, J. M., Gultekin, K., Walton, D. J., Fabian, A. C., Reynolds, C. S., & Nandra, K. 2013, *ApJ*, 771, 1
- King, A., & Nealon, R. 2019, *MNRAS*, 487, 4827
- King, A., & Pounds, K. 2015, *ARA&A*, 53, 115
- King, A. R., & Pringle, J. E. 2006, *MNRAS*, 373, 90
- King, A. R., & Pringle, J. E. 2007, *MNRAS*, 377, L25
- King, A. R., Pringle, J. E., & Hofmann, J. A. 2008, *MNRAS*, 385, 1621
- Koide S., Meier D. L., Shibata K., Kudoh T., 2000, *ApJ*, 536, 668
- Kolos, M., Tursunov, A. & Stuchlik, Z. 2021, *PhRvD*, 103, 024021
- Komissarov S. S., McKinney J. C., 2007, *MNRAS*, 377, L49
- Kormendy, J., & Ho, L. C. 2013, *ARA&A*, 51, 511
- Kormendy, J., & Richstone, D. 1995, *ARA&A*, 33, 581
- Krause, M. G. H., Shabala, S. S., Hardcastle, M. J., Bicknell, G. V., Böhringer, H., Chon, G., Nawaz, M. A., Sarzi, M., Wagner, A. Y. 2019, *MNRAS*, 482, 240
- Kulier, A., Ostriker, J. P., Natarajan, P., Lackner, C. N., & Cen, R. 2015, *ApJ*, 799, 178
- Laing, R. A., Riley, J. M., & Longair, M. S. 1983, *MNRAS*, 204, 151
- Leahy, J. P., Muxlow, T. W. B., & Stephens, P. W. 1989, *MNRAS*, 239, 401
- MacDonald, D., & Thorne, K. S. 1982, *MNRAS*, 198, 345
- McLure, R. J., Jarvis, M. J., Targett, T. A., Dunlop, J. S., & Best, P. N. 2006, *MNRAS*, 368, 1395
- McLure, R. J., Willott, C. J., Jarvis, M. J., et al. 2004, *MNRAS*, 351, 347
- McNamara, B. R., Kazemzadeh, F., Rafferty, D. A., Birzan, L., Nulsen, P. E. J., Kirkpatrick, C. C., Wise, M. W. 2009, *ApJ*, 698, 594
- Meier, D. L. 1999, *ApJ*, 522, 753
- Merloni A., Heinz S., & di Matteo T., 2003, *MNRAS*, 345, 1057
- Mikhailov, A. G. & Gnedin, Y. N., 2018, *Astronomy Reports*, 62, 1
- Mikhailov, A. G., Gnedin, Y. N., & Belonovsky, A. V. 2015, *Astrophysics*, Vol. 58, No. 2, 157
- Mikhailov, A. G., Piotrovich, M. Yu., Buliga, S. D., Natsvlshvili, T. M., Gnedin, Yu. N. 2019, *ARep* 63,433
- Miller, J. M., Fabian, A. C., Wijnands, R., Reynolds, C. S., Ehle, M., Freyberg, M. J., van der Klis, M., Lewin, W. H. G., Sanchez-Fernandez, C., Castro-Tirado, A. J., 2002, *ApJ*, 570, L69
- Miller, J. M., Reynolds, C. S., Fabian, A. C., Miniutti, G., & Gallo, L. C. 2009, *ApJ*, 697, 900
- Misner, C. W., Thorne, K. S., & Wheeler, J. A. 1973, "Gravitation" (San Francisco: W.H. Freeman and Co.)
- Moderski, R., Sikora, M., & Lasota, J.-P. 1998, *MNRAS*, 301, 142
- Nisbet, D. M., & Best, P. N. 2016, *MNRAS*, 455, 2551
- O’Dea, C. P., Daly, R. A., Freeman, K. A., Kharb, P., & Baum, S. 2009, *A&A*, 494, 471
- Patrick, A. R., Reeves, J. N., Porquet, D., Markowitz, A. G., Braitto, V., & Lobban, A. P. 2012, *MNRAS*, 426, 2522
- Penrose, R. 1969, *Riv. Nuovo Cim.*, 1, 252
- Penrose, R., & Floyd, R. M. 1971, *NPhS*, 229, 177
- Phinney, E. S. 1983, *Dissertation University of Cambridge*
- Piotrovich, M. Yu., Afanasiev, V. L., Buliga, S. D., & Natsvlshvili, T. M. 2020, *IJMPA*, 35, 2040054
- Piotrovich, M. Y., Gnedin, Y. N., Natsvlshvili, T. M., & Buliga, S. D. 2017, *Ap&SS*, 362, 231
- Pugliese, D., & Quevedo, H. 2022, *EPJC*, 82, 456 (arXiv:2202.31096)
- Pugliese, D., & Stuchlík, Z. 2021, *Class. Quantum Grav.* 38, 145014

- Punsly, B. 2001, "Black hole gravitohydromagnetics" (New York: Springer)
- Rees, M. J. 1984, *ARA&A*, 22, 471
- Reynolds, C. S. 2019, *Nature Astronomy*, 3, 41
- Saikia P., K rding E., & Falcke H., 2015, *MNRAS*, 450, 2317
- Sesana, A., Barausse, E., Doti, M., & Rossi, E. M. 2014, *ApJ*, 794, 104
- Shabala, S. S., Jurlin, N., Morganti, R., Brienza, M., Hardcastle, M. J., Godfrey, L. E. H., Krause, M. G. H., & Turner, Ross J. 2020, arXiv:2004.08979
- Shankar, F. 2013, *CQGra*, 30, 244001
- Sun, W. H., Malkan, M. A., 1989, *ApJ*, 346, 68
- Tchekhovskoy, A., Narayan, R., McKinney, J. C. 2010, *ApJ*, 711, 50
- Thorne, K. S., Price, R. H., Macdonald, D. A., Wai-Mo, S., & Zhang, X 1986, in "Black Holes: The Membrane Paradigm," 67
- Trakhtenbrot, B. 2014, *ApJ*, 789, L9
- Trakhtenbrot, B., Volonteri, M., Natarajan, P. 2014, *ApJ*, 836, L1
- Vasudevan, R. V., Fabian, A. C., Reynolds, C. S., Aird, J., Dauser, T., & Gallo, L. C. 2016, *MNRAS*, 458, 2012
- Voit, G. M., Donahue, M., Bryan, G. L., & McDonald, M. 2015, *Nature*, 519, 203
- Volonteri, M., Madau, P., Quataert, E., Rees, M. J. 2005, *ApJ*, 620, 69
- Volonteri, M., Sikora, M., & Lasota, J. 2007, *ApJ*, 667, 704
- Volonteri, M., Sikora, M., Lasota, J. -P., & Merloni, A. 2013, *ApJ*, 775, 94
- Walton, D. J., Nardini, E., Fabian, A. C., Gallo, L. C., & Reis 2013, *MNRAS*, 428, 2901
- Wan, L., Daly, R. A., & Guerra, E. J. 2000, *ApJ*, 544, 671
- Wang, J.-M., Du, P., Li, Y.-R., Ho, L. C., Hu, C., Bai, J.-M. 2014, *ApJ*, 792, L13
- Worrall, D. M. 2009, *A&AR*, 17, 1
- Wu, S., Lu, Y., Zhang, F., Lu, Y. 2013, *MNRAS*, 436, 3271
- Yuan, F., & Narayan, R. 2014, *ARA&A*, 52, 529
- Zubovas, K., & King, A. R. 2012, *MNRAS*, 426, 2751
- Zubovas, K., & King, A. R. 2019, *MNRAS*, 489, 1373

This paper has been typeset from a $\text{\TeX}/\text{\LaTeX}$ file prepared by the author.

Table 1. Outflow and Spin Properties for FR II LEG, Q, & W Sources

(1) Source	(2) Type	(3) z	(4) Log (F)	(5) Log ($E_{\text{spin}}/E_{\text{s,max}}$)	(6) Log ($M_{\text{dyn}}/M_{\text{irr}}$)	(7) Log ($M_{\text{spin}}/M_{\text{dyn}}$)	(8) Log ($M_{\text{spin}}/M_{\text{irr}}$)	(9) Log(M_{spin}) (M_{\odot})	(10) Log ($E_{\text{T}}/E_{\text{spin}}$)	(11) Log ($E_{\text{T}}/M_{\text{dyn}}$)
3C 33	HEG	0.059	-0.42 ± 0.18	-0.77 ± 0.35	0.03 ± 0.02	-1.18 ± 0.33	-1.15 ± 0.35	7.38 ± 0.12	-1.40 ± 0.22	-2.58 ± 0.31
3C 192	HEG	0.059	-0.45 ± 0.21	-0.83 ± 0.40	0.03 ± 0.02	-1.24 ± 0.38	-1.22 ± 0.40	7.17 ± 0.12	-1.35 ± 0.24	-2.59 ± 0.32
3C 285	HEG	0.079	-0.30 ± 0.21	-0.54 ± 0.39	0.05 ± 0.04	-0.97 ± 0.35	-0.92 ± 0.39	7.56 ± 0.13	-1.74 ± 0.24	-2.71 ± 0.32
3C 452	HEG	0.081	-0.22 ± 0.17	-0.39 ± 0.31	0.07 ± 0.05	-0.84 ± 0.27	-0.78 ± 0.31	7.87 ± 0.14	-1.76 ± 0.22	-2.61 ± 0.30
3C 388	HEG	0.09	-0.15 ± 0.18	-0.26 ± 0.33	0.09 ± 0.06	-0.73 ± 0.27	-0.65 ± 0.33	8.11 ± 0.15	-2.10 ± 0.24	-2.84 ± 0.31
3C 321	HEG	0.096	-0.59 ± 0.19	-1.10 ± 0.38	0.01 ± 0.01	-1.50 ± 0.37	-1.49 ± 0.38	7.29 ± 0.12	-1.37 ± 0.23	-2.87 ± 0.32
3C 433	HEG	0.101	-0.05 ± 0.16	-0.08 ± 0.27	0.13 ± 0.07	-0.59 ± 0.20	-0.46 ± 0.27	8.37 ± 0.16	-2.18 ± 0.23	-2.77 ± 0.30
3C 20	HEG	0.174	0.14 ± 0.14	0.23 ± 0.22	0.23 ± 0.09	-0.39 ± 0.13	-0.16 ± 0.22	8.19 ± 0.19	-1.84 ± 0.24	-2.23 ± 0.30
3C 28	HEG	0.195	-0.23 ± 0.15	-0.41 ± 0.29	0.07 ± 0.04	-0.86 ± 0.25	-0.79 ± 0.29	8.02 ± 0.14	-1.78 ± 0.21	-2.64 ± 0.30
3C 349	HEG	0.205	-0.08 ± 0.16	-0.14 ± 0.28	0.12 ± 0.06	-0.63 ± 0.21	-0.52 ± 0.28	7.92 ± 0.16	-1.72 ± 0.23	-2.35 ± 0.30
3C 436	HEG	0.214	-0.11 ± 0.15	-0.19 ± 0.27	0.10 ± 0.06	-0.68 ± 0.21	-0.57 ± 0.26	8.18 ± 0.16	-1.90 ± 0.22	-2.57 ± 0.30
3C 171	HEG	0.238	-0.20 ± 0.14	-0.35 ± 0.26	0.07 ± 0.04	-0.80 ± 0.22	-0.73 ± 0.26	7.79 ± 0.15	-1.45 ± 0.21	-2.25 ± 0.30
3C 284	HEG	0.239	-0.30 ± 0.15	-0.55 ± 0.29	0.05 ± 0.03	-0.98 ± 0.26	-0.93 ± 0.29	7.91 ± 0.14	-1.66 ± 0.21	-2.64 ± 0.30
3C 300	HEG	0.27	-0.08 ± 0.14	-0.14 ± 0.25	0.12 ± 0.06	-0.63 ± 0.19	-0.52 ± 0.25	7.92 ± 0.16	-1.55 ± 0.22	-2.18 ± 0.30
3C 438	HEG	0.29	0.12 ± 0.12	0.20 ± 0.20	0.22 ± 0.08	-0.40 ± 0.12	-0.18 ± 0.20	8.71 ± 0.19	-2.14 ± 0.24	-2.54 ± 0.30
3C 299	HEG	0.367	-0.18 ± 0.14	-0.33 ± 0.25	0.08 ± 0.04	-0.79 ± 0.21	-0.71 ± 0.25	7.79 ± 0.15	-1.37 ± 0.21	-2.16 ± 0.31
3C 42	HEG	0.395	-0.05 ± 0.13	-0.08 ± 0.23	0.13 ± 0.06	-0.59 ± 0.17	-0.46 ± 0.23	8.35 ± 0.17	-1.90 ± 0.22	-2.49 ± 0.31
3C 16	HEG	0.405	0.06 ± 0.13	0.10 ± 0.22	0.18 ± 0.08	-0.46 ± 0.14	-0.28 ± 0.22	8.20 ± 0.19	-1.78 ± 0.24	-2.20 ± 0.31
3C 274.1	HEG	0.422	0.20 ± 0.13	0.32 ± 0.20	0.27 ± 0.09	-0.33 ± 0.10	-0.06 ± 0.20	8.60 ± 0.21	-2.06 ± 0.25	-2.39 ± 0.31
3C 457	HEG	0.428	-0.37 ± 0.13	-0.07 ± 0.23	0.04 ± 0.02	-1.09 ± 0.23	-1.05 ± 0.25	7.72 ± 0.14	-1.20 ± 0.20	-2.62 ± 0.33
3C 244.1	HEG	0.428	-0.04 ± 0.13	-0.67 ± 0.25	0.13 ± 0.06	-0.58 ± 0.17	-0.45 ± 0.23	8.40 ± 0.19	-2.04 ± 0.23	-2.28 ± 0.31
3C 46	HEG	0.437	-0.24 ± 0.13	-0.44 ± 0.25	0.06 ± 0.03	-0.88 ± 0.21	-0.82 ± 0.25	8.31 ± 0.15	-1.82 ± 0.21	-2.70 ± 0.31
3C 341	HEG	0.448	-0.19 ± 0.13	-0.34 ± 0.24	0.08 ± 0.04	-0.80 ± 0.20	-0.73 ± 0.24	8.22 ± 0.16	-1.72 ± 0.22	-2.53 ± 0.31
3C 172	HEG	0.519	-0.18 ± 0.13	-0.31 ± 0.24	0.08 ± 0.04	-0.77 ± 0.20	-0.69 ± 0.24	8.12 ± 0.17	-1.58 ± 0.22	-2.35 ± 0.33
3C 330	HEG	0.549	-0.14 ± 0.13	-0.24 ± 0.24	0.09 ± 0.05	-0.72 ± 0.19	-0.62 ± 0.24	8.39 ± 0.18	-1.65 ± 0.24	-2.37 ± 0.34
3C 49	HEG	0.621	-0.11 ± 0.13	0.05 ± 0.20	0.10 ± 0.05	-0.67 ± 0.18	-0.57 ± 0.23	8.44 ± 0.18	-1.83 ± 0.23	-2.50 ± 0.33
3C 337	HEG	0.635	0.01 ± 0.13	-0.18 ± 0.23	0.15 ± 0.07	-0.53 ± 0.16	-0.37 ± 0.22	8.43 ± 0.20	-1.99 ± 0.24	-2.51 ± 0.33
3C 34	HEG	0.69	-0.32 ± 0.12	0.01 ± 0.22	0.05 ± 0.02	-1.01 ± 0.21	-0.96 ± 0.23	8.21 ± 0.16	-1.51 ± 0.22	-2.51 ± 0.34
3C 441	HEG	0.708	-0.02 ± 0.13	-0.58 ± 0.23	0.14 ± 0.06	-0.56 ± 0.16	-0.42 ± 0.22	8.68 ± 0.20	-1.98 ± 0.25	-2.54 ± 0.34
3C 247	HEG	0.749	-0.36 ± 0.13	-0.04 ± 0.22	0.04 ± 0.02	-1.07 ± 0.23	-1.03 ± 0.26	8.34 ± 0.16	-1.78 ± 0.22	-2.85 ± 0.34
3C 277.2	HEG	0.766	-0.11 ± 0.13	0.38 ± 0.20	0.10 ± 0.05	-0.67 ± 0.18	-0.57 ± 0.22	8.36 ± 0.19	-1.60 ± 0.24	-2.28 ± 0.35
3C 340	HEG	0.775	-0.03 ± 0.13	-0.65 ± 0.26	0.14 ± 0.06	-0.56 ± 0.16	-0.43 ± 0.22	8.47 ± 0.20	-1.77 ± 0.25	-2.34 ± 0.34
3C 352	HEG	0.806	-0.17 ± 0.13	-0.19 ± 0.22	0.08 ± 0.04	-0.77 ± 0.19	-0.69 ± 0.23	8.43 ± 0.18	-1.67 ± 0.23	-2.44 ± 0.35
3C 263.1	HEG	0.824	-0.02 ± 0.13	-0.04 ± 0.22	0.14 ± 0.06	-0.56 ± 0.16	-0.42 ± 0.22	8.71 ± 0.21	-1.86 ± 0.26	-2.42 ± 0.35
3C 217	HEG	0.897	0.06 ± 0.13	-0.30 ± 0.23	0.18 ± 0.07	-0.47 ± 0.14	-0.29 ± 0.21	8.35 ± 0.23	-1.56 ± 0.27	-2.03 ± 0.36
3C 175.1	HEG	0.92	0.08 ± 0.13	-0.03 ± 0.22	0.19 ± 0.08	-0.45 ± 0.14	-0.25 ± 0.21	8.64 ± 0.23	-1.82 ± 0.28	-2.27 ± 0.36
3C 289	HEG	0.967	0.03 ± 0.14	0.09 ± 0.21	0.17 ± 0.07	-0.50 ± 0.15	-0.33 ± 0.23	8.93 ± 0.23	-2.17 ± 0.28	-2.67 ± 0.37
3C 280	HEG	0.996	-0.44 ± 0.14	0.13 ± 0.21	0.03 ± 0.02	-1.22 ± 0.26	-1.19 ± 0.27	8.21 ± 0.17	-1.55 ± 0.23	-2.77 ± 0.37
3C 356	HEG	1.079	0.08 ± 0.15	0.05 ± 0.23	0.20 ± 0.09	-0.44 ± 0.15	-0.24 ± 0.24	9.01 ± 0.25	-2.01 ± 0.31	-2.45 ± 0.39
3C 252	HEG	1.103	-0.04 ± 0.13	-0.81 ± 0.27	0.13 ± 0.06	-0.58 ± 0.17	-0.45 ± 0.23	8.72 ± 0.22	-1.81 ± 0.27	-2.39 ± 0.38
3C 368	HEG	1.132	-0.01 ± 0.14	0.14 ± 0.24	0.14 ± 0.07	-0.55 ± 0.17	-0.41 ± 0.23	8.90 ± 0.23	-1.91 ± 0.28	-2.46 ± 0.39
3C 267	HEG	1.14	0.02 ± 0.14	-0.06 ± 0.23	0.16 ± 0.07	-0.52 ± 0.17	-0.36 ± 0.24	8.87 ± 0.24	-1.94 ± 0.29	-2.45 ± 0.39
3C 324	HEG	1.206	-0.12 ± 0.15	-0.02 ± 0.23	0.10 ± 0.06	-0.69 ± 0.22	-0.59 ± 0.27	8.87 ± 0.22	-1.99 ± 0.28	-2.68 ± 0.40
3C 266	HEG	1.275	-0.08 ± 0.14	0.03 ± 0.24	0.11 ± 0.06	-0.64 ± 0.19	-0.52 ± 0.24	8.73 ± 0.23	-1.77 ± 0.28	-2.40 ± 0.40
3C 13	HEG	1.351	-0.05 ± 0.14	-0.21 ± 0.27	0.13 ± 0.06	-0.59 ± 0.18	-0.46 ± 0.24	9.01 ± 0.24	-2.01 ± 0.29	-2.60 ± 0.41
4C 13.66	HEG	1.45	0.08 ± 0.14	-0.14 ± 0.24	0.19 ± 0.08	-0.44 ± 0.15	-0.25 ± 0.23	8.75 ± 0.27	-1.75 ± 0.32	-2.20 ± 0.42
3C 437	HEG	1.48	0.31 ± 0.15	-0.08 ± 0.24	0.36 ± 0.12	-0.25 ± 0.09	0.10 ± 0.21	9.13 ± 0.32	-1.91 ± 0.37	-2.16 ± 0.43
3C 241	HEG	1.617	0.03 ± 0.15	0.13 ± 0.23	0.16 ± 0.08	-0.50 ± 0.17	-0.34 ± 0.25	9.07 ± 0.27	-1.99 ± 0.32	-2.49 ± 0.44
3C 470	HEG	1.653	0.19 ± 0.15	0.49 ± 0.21	0.27 ± 0.11	-0.34 ± 0.12	-0.07 ± 0.23	9.11 ± 0.31	-2.08 ± 0.35	-2.42 ± 0.44
3C 322	HEG	1.681	0.29 ± 0.16	-0.08 ± 0.27	0.34 ± 0.12	-0.27 ± 0.10	0.07 ± 0.23	9.24 ± 0.33	-2.09 ± 0.38	-2.36 ± 0.45
3C 239	HEG	1.781	0.17 ± 0.16	0.04 ± 0.25	0.25 ± 0.11	-0.36 ± 0.14	-0.11 ± 0.26	9.21 ± 0.32	-2.07 ± 0.37	-2.43 ± 0.46
3C 294	HEG	1.786	0.05 ± 0.16	0.31 ± 0.23	0.18 ± 0.09	-0.48 ± 0.17	-0.30 ± 0.26	8.98 ± 0.29	-1.87 ± 0.34	-2.34 ± 0.46
3C 225B	HEG	0.582	0.03 ± 0.12	0.45 ± 0.23	0.17 ± 0.07	-0.50 ± 0.14	-0.33 ± 0.21	8.50 ± 0.20	-1.77 ± 0.25	-2.27 ± 0.33
3C 55	HEG	0.735	0.24 ± 0.13	0.27 ± 0.26	0.30 ± 0.10	-0.30 ± 0.10	0.00 ± 0.20	8.86 ± 0.24	-1.94 ± 0.29	-2.24 ± 0.35
3C 68.2	HEG	1.575	-0.04 ± 0.16	0.08 ± 0.26	0.13 ± 0.07	-0.59 ± 0.20	-0.46 ± 0.27	8.95 ± 0.25	-2.00 ± 0.30	-2.59 ± 0.44

Table 2. Outflow and Spin Properties for FR II LEG, Q, & W Sources

(1) Source	(2) Type	(3) z	(4) Log (F)	(5) Log ($E_{\text{spin}}/E_{\text{spin,max}}$)	(6) Log ($M_{\text{dyn}}/M_{\text{irr}}$)	(7) Log ($M_{\text{spin}}/M_{\text{dyn}}$)	(8) Log ($M_{\text{spin}}/M_{\text{irr}}$)	(9) Log(M_{spin}) (M_{\odot})	(10) Log ($E_{\text{T}}/E_{\text{spin}}$)	(11) Log ($E_{\text{T}}/M_{\text{dyn}}$)
3C 35	LEG	0.067	-0.25 ± 0.22	-0.46 ± 0.41	0.06 ± 0.05	-0.90 ± 0.36	-0.84 ± 0.41	7.75 ± 0.14	-2.01 ± 0.26	-2.91 ± 0.33
3C 326	LEG	0.088	-0.09 ± 0.19	-0.16 ± 0.33	0.11 ± 0.07	-0.65 ± 0.26	-0.54 ± 0.33	7.73 ± 0.15	-1.77 ± 0.24	-2.42 ± 0.31
3C 236	LEG	0.099	-0.20 ± 0.19	-0.36 ± 0.35	0.07 ± 0.05	-0.82 ± 0.30	-0.75 ± 0.35	7.99 ± 0.14	-2.06 ± 0.24	-2.88 ± 0.32
4C 12.03	LEG	0.156	-0.19 ± 0.18	-0.33 ± 0.32	0.08 ± 0.05	-0.79 ± 0.27	-0.71 ± 0.32	8.06 ± 0.14	-2.01 ± 0.22	-2.80 ± 0.31
3C 319	LEG	0.192	0.10 ± 0.16	0.17 ± 0.25	0.21 ± 0.10	-0.42 ± 0.16	-0.21 ± 0.25	7.90 ± 0.18	-1.69 ± 0.24	-2.11 ± 0.30
3C 132	LEG	0.214	-0.17 ± 0.15	-0.31 ± 0.28	0.08 ± 0.05	-0.77 ± 0.23	-0.69 ± 0.28	7.97 ± 0.15	-1.74 ± 0.22	-2.51 ± 0.30
3C 123	LEG	0.218	0.31 ± 0.12	0.49 ± 0.17	0.36 ± 0.09	-0.25 ± 0.07	0.11 ± 0.17	8.57 ± 0.21	-1.86 ± 0.26	-2.11 ± 0.30
3C 153	LEG	0.277	-0.21 ± 0.14	-0.38 ± 0.26	0.07 ± 0.04	-0.83 ± 0.22	-0.76 ± 0.26	8.11 ± 0.15	-1.76 ± 0.21	-2.59 ± 0.30
4C 14.27	LEG	0.392	0.03 ± 0.14	0.06 ± 0.23	0.17 ± 0.07	-0.49 ± 0.15	-0.33 ± 0.23	8.24 ± 0.19	-1.79 ± 0.24	-2.28 ± 0.31
3C 200	LEG	0.458	-0.09 ± 0.13	-0.15 ± 0.23	0.11 ± 0.05	-0.65 ± 0.18	-0.54 ± 0.23	8.30 ± 0.17	-1.79 ± 0.22	-2.43 ± 0.31
3C 295	LEG	0.461	0.23 ± 0.12	0.37 ± 0.18	0.29 ± 0.09	-0.31 ± 0.09	-0.02 ± 0.18	9.15 ± 0.22	-2.29 ± 0.27	-2.60 ± 0.32
3C 19	LEG	0.482	-0.14 ± 0.13	-0.24 ± 0.23	0.09 ± 0.05	-0.72 ± 0.19	-0.63 ± 0.23	8.44 ± 0.17	-1.91 ± 0.22	-2.63 ± 0.32
3C 427.1	LEG	0.572	-0.24 ± 0.13	-0.44 ± 0.24	0.06 ± 0.03	-0.88 ± 0.21	-0.82 ± 0.24	8.28 ± 0.16	-1.74 ± 0.21	-2.62 ± 0.33
3C 249.1	Q	0.311	-0.56 ± 0.17	-1.04 ± 0.33	0.02 ± 0.01	-1.44 ± 0.31	-1.42 ± 0.33	7.86 ± 0.19	-1.53 ± 0.24	-2.96 ± 0.43
3C 351	Q	0.371	-0.38 ± 0.16	-0.70 ± 0.30	0.04 ± 0.02	-1.12 ± 0.28	-1.08 ± 0.30	8.38 ± 0.20	-1.94 ± 0.25	-3.05 ± 0.43
3C 215	Q	0.411	0.04 ± 0.16	0.07 ± 0.26	0.17 ± 0.09	-0.49 ± 0.18	-0.32 ± 0.26	7.81 ± 0.27	-1.33 ± 0.31	-1.82 ± 0.43
3C 47	Q	0.425	-0.20 ± 0.15	-0.36 ± 0.27	0.07 ± 0.04	-0.82 ± 0.23	-0.75 ± 0.27	8.38 ± 0.22	-1.74 ± 0.26	-2.56 ± 0.42
3C 334	Q	0.555	-0.31 ± 0.15	-0.57 ± 0.28	0.05 ± 0.03	-0.99 ± 0.25	-0.95 ± 0.28	8.71 ± 0.21	-2.01 ± 0.26	-3.01 ± 0.43
3C 275.1	Q	0.557	-0.26 ± 0.15	-0.46 ± 0.29	0.06 ± 0.04	-0.90 ± 0.25	-0.84 ± 0.29	7.40 ± 0.22	-1.13 ± 0.26	-2.03 ± 0.42
3C 263	Q	0.646	-0.20 ± 0.14	-0.35 ± 0.27	0.07 ± 0.04	-0.81 ± 0.23	-0.74 ± 0.27	8.29 ± 0.23	-1.58 ± 0.27	-2.39 ± 0.43
3C 207	Q	0.684	0.12 ± 0.14	0.20 ± 0.23	0.22 ± 0.09	-0.40 ± 0.14	-0.18 ± 0.23	8.10 ± 0.29	-1.38 ± 0.33	-1.78 ± 0.43
3C 254	Q	0.734	-0.27 ± 0.15	-0.49 ± 0.29	0.06 ± 0.03	-0.93 ± 0.26	-0.87 ± 0.29	8.37 ± 0.21	-1.68 ± 0.26	-2.60 ± 0.43
3C 175	Q	0.768	-0.15 ± 0.15	-0.27 ± 0.26	0.09 ± 0.05	-0.74 ± 0.22	-0.65 ± 0.27	9.16 ± 0.23	-2.31 ± 0.28	-3.05 ± 0.43
3C 196	Q	0.871	0.19 ± 0.15	0.31 ± 0.23	0.27 ± 0.11	-0.34 ± 0.12	-0.07 ± 0.23	9.26 ± 0.31	-2.16 ± 0.36	-2.50 ± 0.44
3C 309.1	Q	0.904	-0.02 ± 0.14	-0.03 ± 0.25	0.14 ± 0.07	-0.56 ± 0.18	-0.41 ± 0.25	8.54 ± 0.26	-1.66 ± 0.30	-2.21 ± 0.43
3C 336	Q	0.927	-0.08 ± 0.14	-0.14 ± 0.25	0.11 ± 0.06	-0.64 ± 0.20	-0.53 ± 0.25	8.56 ± 0.25	-1.76 ± 0.29	-2.40 ± 0.43
3C 245	Q	1.029	-0.06 ± 0.14	-0.10 ± 0.25	0.12 ± 0.06	-0.61 ± 0.19	-0.48 ± 0.25	8.79 ± 0.25	-1.90 ± 0.30	-2.51 ± 0.43
3C 212	Q	1.049	0.04 ± 0.14	0.07 ± 0.24	0.17 ± 0.08	-0.49 ± 0.16	-0.32 ± 0.24	8.71 ± 0.27	-1.79 ± 0.31	-2.27 ± 0.43
3C 186	Q	1.063	-0.10 ± 0.14	-0.17 ± 0.26	0.11 ± 0.06	-0.66 ± 0.20	-0.56 ± 0.26	8.84 ± 0.24	-1.89 ± 0.29	-2.55 ± 0.43
3C 208	Q	1.11	0.04 ± 0.15	0.06 ± 0.24	0.17 ± 0.08	-0.49 ± 0.16	-0.32 ± 0.24	8.91 ± 0.27	-1.93 ± 0.32	-2.42 ± 0.43
3C 204	Q	1.112	0.00 ± 0.14	0.00 ± 0.24	0.15 ± 0.07	-0.54 ± 0.17	-0.39 ± 0.24	8.96 ± 0.26	-2.06 ± 0.30	-2.59 ± 0.43
3C 190	Q	1.197	0.20 ± 0.15	0.32 ± 0.22	0.27 ± 0.10	-0.33 ± 0.12	-0.06 ± 0.22	8.37 ± 0.31	-1.38 ± 0.35	-1.71 ± 0.43
3C 68.1	Q	1.238	0.06 ± 0.15	0.09 ± 0.25	0.18 ± 0.08	-0.47 ± 0.16	-0.29 ± 0.25	9.43 ± 0.28	-2.33 ± 0.33	-2.80 ± 0.44
4C 16.49	Q	1.296	-0.06 ± 0.14	-0.10 ± 0.25	0.13 ± 0.06	-0.60 ± 0.19	-0.48 ± 0.25	9.20 ± 0.25	-2.23 ± 0.30	-2.83 ± 0.43
3C 181	Q	1.382	-0.14 ± 0.15	-0.25 ± 0.27	0.09 ± 0.05	-0.72 ± 0.22	-0.63 ± 0.27	8.88 ± 0.24	-1.82 ± 0.30	-2.55 ± 0.44
3C 268.4	Q	1.4	0.03 ± 0.18	0.05 ± 0.30	0.17 ± 0.10	-0.50 ± 0.20	-0.33 ± 0.30	9.30 ± 0.27	-2.05 ± 0.34	-2.55 ± 0.45
3C 14	Q	1.469	-0.04 ± 0.15	-0.07 ± 0.25	0.13 ± 0.07	-0.59 ± 0.19	-0.46 ± 0.25	8.81 ± 0.26	-1.82 ± 0.31	-2.41 ± 0.43
3C 270.1	Q	1.519	0.41 ± 0.15	0.62 ± 0.21	0.44 ± 0.13	-0.20 ± 0.08	0.24 ± 0.21	8.80 ± 0.34	-1.56 ± 0.39	-1.76 ± 0.44
3C 205	Q	1.534	-0.06 ± 0.15	-0.10 ± 0.26	0.12 ± 0.06	-0.61 ± 0.19	-0.49 ± 0.26	8.99 ± 0.25	-1.94 ± 0.30	-2.55 ± 0.44
3C 432	Q	1.805	-0.07 ± 0.15	-0.11 ± 0.26	0.12 ± 0.06	-0.62 ± 0.20	-0.50 ± 0.26	9.48 ± 0.25	-2.37 ± 0.31	-2.98 ± 0.44
3C 191	Q	1.956	-0.01 ± 0.15	-0.01 ± 0.26	0.15 ± 0.08	-0.54 ± 0.19	-0.39 ± 0.26	9.16 ± 0.26	-1.98 ± 0.32	-2.52 ± 0.44
3C 9	Q	2.012	0.14 ± 0.16	0.24 ± 0.25	0.23 ± 0.11	-0.38 ± 0.15	-0.15 ± 0.25	9.42 ± 0.30	-2.14 ± 0.36	-2.52 ± 0.45
3C 223	W	0.136	-0.36 ± 0.17	-0.65 ± 0.33	0.04 ± 0.03	-1.07 ± 0.30	-1.03 ± 0.33	7.41 ± 0.13	-1.34 ± 0.22	-2.41 ± 0.31
3C 79	W	0.255	-0.12 ± 0.13	-0.22 ± 0.24	0.10 ± 0.05	-0.70 ± 0.19	-0.60 ± 0.24	8.09 ± 0.16	-1.63 ± 0.22	-2.33 ± 0.30
3C 109	W	0.305	-0.14 ± 0.16	-0.25 ± 0.28	0.09 ± 0.05	-0.72 ± 0.23	-0.63 ± 0.28	7.58 ± 0.24	-1.12 ± 0.28	-1.84 ± 0.43

Table 3. Unweighted Mean Value and Standard Deviation of Black Hole Spin Mass-Energy Parameters (top five rows; values in parentheses indicate the average uncertainty per source), and Unweighted Best Fit Values to Each Quantity vs. $\text{Log}(1+z)$ (bottom three rows).

(1)	(2)	(3)	(4)	(5)	(6)	(7)	(8)	(9)
	N	Log ($M_{\text{dyn}}/M_{\text{irr}}$)	Log ($M_{\text{spin}}/M_{\text{dyn}}$)	Log ($M_{\text{spin}}/M_{\text{irr}}$) ^a	Log ($M_{\text{spin}}/M_{\odot}$)	Log (F)	Log ($E_{\text{T}}/E_{\text{spin}}$)	Log ($E_{\text{T}}/M_{\text{dyn}}$)
HEG	55	0.13 ± 0.08(0.06)	-0.66 ± 0.27(0.19)	-0.53 ± 0.34(0.25)	8.41 ± 0.50(0.25)	-0.08 ± 0.19(0.14)	-1.80 ± 0.23(0.30)	-2.46 ± 0.19(0.35)
Q	29	0.14 ± 0.09(0.07)	-0.64 ± 0.26(0.19)	-0.50 ± 0.34(0.26)	8.72 ± 0.52(0.26)	-0.06 ± 0.19(0.15)	-1.84 ± 0.31(0.31)	-2.48 ± 0.38(0.43)
LEG	13	0.14 ± 0.10(0.06)	-0.65 ± 0.22(0.21)	-0.52 ± 0.31(0.27)	8.19 ± 0.38(0.27)	-0.07 ± 0.18(0.15)	-1.88 ± 0.17(0.31)	-2.53 ± 0.26(0.31)
W	3	0.08 ± 0.03(0.04)	-0.83 ± 0.21(0.24)	-0.75 ± 0.24(0.28)	7.69 ± 0.35(0.28)	-0.21 ± 0.13(0.15)	-1.37 ± 0.26(0.32)	-2.19 ± 0.31(0.34)
All	100	0.13 ± 0.08(0.06)	-0.66 ± 0.26(0.20)	-0.53 ± 0.33(0.26)	8.45 ± 0.53(0.26)	-0.08 ± 0.19(0.15)	-1.81 ± 0.26(0.30)	-2.47 ± 0.27(0.37)
Slope	100	0.28 ± 0.06	0.97 ± 0.18	1.25 ± 0.23	3.46 ± 0.23	0.71 ± 0.13	-0.73 ± 0.19	0.25 ± 0.22
Y-int	100	0.07 ± 0.02	-0.88 ± 0.05	-0.80 ± 0.06	7.68 ± 0.06	-0.23 ± 0.03	-1.65 ± 0.05	-2.52 ± 0.06
χ^2	100	0.54	4.96	8.33	8.52	2.71	5.95	7.27

^a $\text{Log}(E_{\text{spin}}/E_{\text{spin,max}}) \approx 0.38 + \text{Log}(M_{\text{spin}}/M_{\text{irr}})$ since $(E_{\text{spin}}/E_{\text{spin,max}}) \approx 2.41(M_{\text{spin}}/M_{\text{irr}})$. This does not affect the standard deviation or average uncertainty per source listed in the top five rows of the table; thus the unweighted mean value of $\text{Log}(E_{\text{spin}}/E_{\text{spin,max}})$ is obtained by adding 0.38 to that listed for $\text{Log}(M_{\text{spin}}/M_{\text{irr}})$, bringing the value for 100 sources to $-0.15 \pm 0.33(0.26)$, for example. It does not affect the slope or χ^2 listed in the bottom part of the table for $\text{Log}(M_{\text{spin}}/M_{\text{irr}})$ though it does add 0.38 to the y-intercept, bringing this value to -0.42 for $\text{Log}(E_{\text{spin}}/E_{\text{spin,max}})$.